DEVELOPMENT OF MAGNETIC-BASED CORE-SHELL NANOPARTICLES FOR DRUG DELIVERY APPLICATION IN MELANOMA SKIN CANCER

by

ZARNA A BHAVSAR

Presented to the Faculty of the Graduate School of

The University of Texas at Arlington in Partial Fulfillment

of the Requirements

for the Degree of

MASTER OF SCIENCE IN BIOMEDICAL ENGINEERING

THE UNIVERSITY OF TEXAS AT ARLINGTON

AUGUST 2010

ACKNOWLEDGEMENTS

First and foremost, I would like to thank Dr. Kytai Truong Nguyen for giving me an opportunity to work in her laboratory for the past two years. I am thankful to her for entrusting me with the responsibility of many exciting and challenging research projects to work on which have helped me improve my research and analytical skills tremendously. Her constant guidance, patience, and encouragement have always inspired me to work hard with sincerity and honesty. Without her immense faith in me I would not have been able to work towards the achievement of my goal.

I would like to thank Dr. Liping Tang for collaborating with us on this project and Dr. Jian Yang for serving on my thesis committee and reviewing my research work. I would like to extend my thanks to Dr. Liping Tang's laboratory members especially Dr. Cheng-Yu Ko and Ashwin Nair for their help with *in vivo* and HPLC studies respectively. Moreover, I would like to recognize our collaborator Dr. Weina Cui for her help on MRI studies. I would also like to take this opportunity to thank Aniket Wadajkar for being a source of motivation and constant support throughout my stay in the lab. I would like to express my deep gratitude to all my laboratory members including Bhanuprasanth Koppolu, Soujanya Kona, Hao Xu, Mandy Su, and Nidhi Singh.

Lastly but most importantly, I remain indebted to my father Mr. Ashwin Bhavsar and my mother Mrs. Nayna Bhavsar for their unconditional love and support throughout my life. Also a special thanks to my sister Jhalak Bhavsar and brother Bhaavan Bhavsar for being supportive, loving, and caring. I would also like to recognize an extraordinary support from my fiancé Aditya Patel throughout my graduate studies.

July 15, 2010

ABSTRACT

DEVELOPMENT OF MAGNETIC-BASED CORE-SHELL NANOPARTICLES FOR DRUG DELIVERY APPLICATION IN MELANOMA SKIN CANCER

Zarna Ashwin Bhavsar, M.S.

The University of Texas at Arlington, 2010

Supervising Professor: Kytai Truong Nguyen

Melanoma skin cancer is the most dangerous form of skin cancer and the major cause of deaths related to skin cancer worldwide. Conventional chemotherapeutic treatment is not very effective and faces many problems such as low response rate, development of multidrug resistance, and severe side effects. In order to address these limitations and improve melanoma treatment efficacy, development of a multifunctional nanoparticulate drug delivery system is desired. Thus, we aimed towards the development of magnetic-based core-shell nanoparticles (MBCS NPs) for dual drug release and dual targeting of melanoma tumors. The synthesized nanoparticles were composed of Poly (Lactic-co-glycolic acid) (PLGA) particle core embedded with functionalized magnetite nanoparticles and a thermo-responsive polymer Poly (N'isopropylacrylamide-acrylamide-allylamine) (PNIPAAm-AAm-AH) shell. The nanoparticles were further conjugated with therapeutic targeting peptide Gly-Arg-Gly-Asp-Ser (GRGDS), which were specifically bound to skin cancer cells, to increase selectivity and efficacy towards melanoma treatment.

The nanoparticles were 300-400 nm in size, which was confirmed by Transmission electron microscopy (TEM) and Dynamic light scattering (DLS) techniques. Their saturation magnetization value measured using SQUID magnetometer was 15.65 emu/g. The nanoparticles exhibited no cytotoxicity towards human dermal fibroblast (HDF)s cells up to a concentration of

500 μg/ml, whereas the optimum nanoparticle concentration uptaken by melanoma cancer (B16F10) cells was about 300 μg/ml. A sustained Curcumin release from the core of the nanoparticles was observed until 25 days, and a burst Doxorubicin release from the thermo-sensitive shell of the nanoparticles at 41˚C was observed over a period of seven days. The developed nanoparticles were also effective for use as contrast agents for MRI. The *in vitro* pharmacological studies indicated the effectiveness of the MBCS NPs loaded with two drugs. The recruitment of the GRGDS-conjugated MBCS NPs at the tumor site was also observed in preliminary *in vivo* studies using animal (mice) models. These results suggest that our nanoparticles can be used as drug carriers to deliver two types of drugs and to specifically deliver these chemotherapeutic reagents to melanoma skin cancer only in order to increase their clinical efficiency and to reduce their severe side effects.

TABLE OF CONTENTS

LIST OF ILLUSTRATIONS

Figure Page

LIST OF TABLES

CHAPTER 1

INTRODUCTION

1.1 Background of skin cancer

Skin is the largest organ of the human body and the most accessible organ to the outer environment. An abnormal growth of cancerous cells superficially on the skin or subcutaneously, which may eventually spread to lymph nodes and migrate to other organs, is referred as skin cancer [1]. The most common cause responsible for the occurrence of skin cancer is the Ultraviolet radiation (UV) from the sun [2, 3]. The risk of skin cancer in any individual, who is exposed to UV radiation especially for prolonged periods of times, is increased [4]. Incidence of skin cancer does have a large dependence on the geographical location and the physical features like skin color, hair color, and eye color of the individual. Other risk factors for skin cancer include precancerous lesions, acute sun burns, exposure to carcinogens, family history of skin cancer, moles present on the body, and adverse environmental conditions [5]. According to the current statistics, skin cancer is the most prevalent form of cancer in the United States [6]. In 2009, about 2 million new cases of Non-Melanoma and 68,720 new cases of Melanoma skin cancer were diagnosed according to the American Cancer Society.

1.1.1 Overview of skin cancer

Skin cancer is normally categorized under two main categories. 1) The non-melanoma skin cancer which occurs in most of the skin cancer patients. It is identified to be of either basal cell origin or squamous cell origin. These cancer types are less dangerous, are localized to the skin, and normally do not spread to other organs, making them easily accessible to surgery and other forms of treatment. 2) The less frequent but more potent form of skin cancer is Melanoma. The melanoma tumor growth starts by mutation in the melanocytes; the pigment producing cells

in our skin. After transformation of the melanocytes, the growth of these cells increases tremendously followed by extensive angiogenesis in the area near the tumor growth. This large mass of blood vessels provides an excellent microenvironment suitable for the growth of tumors. The tumor cells easily penetrate the lymphatic vessels and the blood vessels, circulate to the distant organs and metastasize. These cancer cells invade various other organs like lymph nodes, lungs, brain, heart, liver to eventually destroy the normal functioning of the human body [7]. Figure 1A and 1B respectively provide a schematic of normal skin structure and types of skin cancer [8].

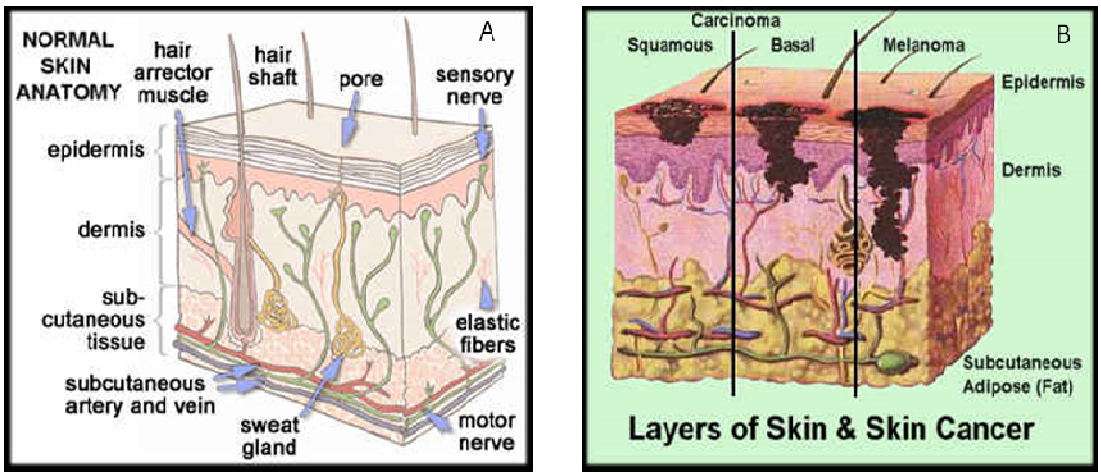

Figure 1.1 (A) Structure of a healthy skin with three main sublayers: epidermis, dermis, and subcutaneous tissues. (B) Types of skin cancer: Squamous cell carcinoma growth starts in the stratum corneum region of the epidermis and may spread to other organs, basal cell carcinoma develops in the basal cells of the epidermis and is less aggressive than squamous cell carcinoma, while the most dangerous form of skin cancer is Melanoma, which initiates in the melanocyte cells of the epidermis and metastasizes to different organs in the body [8].

1.1.2 Current cancer treatment methods and limitations

Conventional treatment methods for skin cancer include surgical excision, chemotherapy, and radiation therapy which are known to possess many side effects and lower the quality of life of the patients. In addition, a low success rate for these treatment methods also causes increasing cases of deaths related to melanoma incidence worldwide [1, 6, 9, 10].

Surgery: Local skin cancer tumors are preferred to be surgically removed as they can be easily operated; and other side effects from toxic drugs or radiation can be avoided. In case of melanoma where the cancerous growth may rapidly spread to the lymph nodes and distant

organs, a biopsy on lymph nodes in the region of tumor is done. If cancerous growth is found, the lymph nodes are also dissected surgically along with the tumors. But removal of the infected lymph nodes causes many long term side effects like poor drainage of fluid and building up of fluid in the arms and legs resulting in the swelling of these body parts.

Chemotherapy: Treating the spreading cancer with chemotherapeutic drugs is another common practice for skin cancer patients, especially those suffering from melanoma. Several drugs or combinations of drugs are used to kill metastasizing skin cancer cells. Intravenous injections or oral chemotherapy is preferred for drug administration. For squamous cell skin cancer, 5-Fluoro uracil (5FU) drug is used in form of topical creams. Currently, drugs like dacarbazine, temozlomide, paclitaxel, doxorubicin, cisplatin, fotemustine, vindesine, and bleomysin are also used for skin cancer treatment. The most important drawback of chemotherapy is that there is a very high chance of developing a multidrug resistance (MDR) effect on the cancer cells after a prolonged treatment. Chemotherapy is also challenged with low response rates and poor survival rates as well as severe side effects such as nausea, hair loss, low immunity, and fatigue.

Immunotherapy: Cytokines, Interferon-alpha, melanoma vaccines, and Imiquimod cream are immunotherapy agents used to treat melanoma. These agents increase the immunity of the patients and help the body fight against the cancer development. This therapy faces several side effects like serious infections and other problems including fever, aches, and feeling sickness.

Radiation therapy: This treatment method is only used when skin cancer tumors cannot be totally removed by surgical excision. The radiation therapy may also be done on the local tumors, lymph nodes, or distant organs like brain. This therapy is useful for shrinking of the tumors; thus reducing the symptoms of the cancer however this therapy does not help much in curing the tumors.

1.2 Nanoparticles for cancer treatment

1.2.1 Ideal nanoparticulate system for cancer treatment

To overcome the limitations of the conventional therapeutics, development of a nanoparticulate-based drug delivery and imaging system with various characteristics is much desired in the field of cancer nanotechnology. Effective melanoma treatment requires a drug delivery system, which can deliver the drug exactly to the site of interest in an optimum dose without causing any harmful effects on the healthy organs [11]. The nanoparticles carrying the therapeutic agent should pass through the whole body, reach to the target site, and be up taken only by cancer cells and/or the tumor tissues [12]. While traversing through the body, the nanoparticles should not be cleared by the macrophages or the Reticuloendothelial system (RES) system before reaching the target site [13]. The release rate of a therapeutic agent present in nanoparticles should be able to be controlled per the requirement. The drug delivery system should be efficient and Multi Drug Resistant (MDR) effect should be minimal [14]. Along with treatment, non invasive monitoring of the location and effectiveness of the drug delivery system should also be helpful [15-17].

The development of the ideal nanoparticulate system is restricted till date due to a number of physiological factors. The nanoparticles that enter the body through an intravenous injection, have to overcome many barriers like the blood brain barrier, vasculature, plasma proteins, extracellular matrices, and non targeted cell surfaces before they can be uptaken by the targeted cells. Even after being uptaken by the target cells, there are intracellular barriers like the nuclear membrane and lysosomal inactivation of the drug to be overcome by the drug carrier [12]. To overcome these physiological restrictions, different types of polymeric and metallic nanoparticles with variable sizes, shapes and surface properties have been developed and investigated. Also, different types of active and passive cancer targeting mechanisms have been employed using nanoparticles [18]. Use of multiple drugs to rapidly and effectively kill the tumor cells without developing the MDR effect has also been studied [14, 19]. The current progress in

the field of cancer nanotechnology using nanoparticles seems to address and overcome a few issues of conventional therapies as listed earlier.

1.2.2 Biodegradable nanoparticles as drug delivery vehicles for cancer treatment

Use of natural and synthetic biodegradable polymers like Poly-lactic acid (PLA), Poly (Lactic-co-glycolic acid (PLGA), chitosan, gelatin, polycaprolactone (PCL), and others for nanoparticle synthesis is widely investigated because polymeric nanoparticles provide an efficient cargo for drug loading and release in a controlled manner. The degradable polymeric nanopaticles have several qualities which make them better cancer treatment options compared to conventional chemotherapy. For example, the delivery of anti-cancer drugs from the degradable nanoparticles increases the bioavailability of the drug at the target site. In addition, small doses of drugs can be used so that the side effects can be reduced. Also, the solubility of the drugs, which are not soluble in the blood plasma, can be increased via nanoparticles [20, 21]. Furthermore, the nanoparticle surface can be modified by various bioactive molecules like proteins, peptides, antibodies, and dendrimers to enhance the particle targeting abilities and particles-cells interactions. The degradable nanoparticles may consist of polymeric matrix or an aqueous core surrounded by a polymeric shell [22]. It is also important to note that not only chemotherapeutic agents but also imaging agents like quantum dots, iron oxide nanoparticles as well as NIRS dyes can be loaded into the polymeric nanoparticles for cancer-based imaging applications in addition to drug delivery applications [23-26].

1.2.3 Magnetic nanoparticles for cancer treatment and imaging

There are a variety of materials like iron, nickel, cobalt, manganese, and their oxides, which are known to possess magnetic properties. Out of these, iron-oxide has a tendency to degrade into non-toxic iron and oxygen components *in vivo* while the other magnetic materials are potentially toxic to the cells, making the iron-oxide-based nanoparticles suitable for nanomedicine applications [13]. In fact, the iron-oxide-based nanoparticles possess extraordinary structural, functional, and optical properties for both therapeutic and diagnostic

applications simultaneously [11]. The two types of iron oxide nanoparticles are magnetite (Fe_3O_4) and maghemite (γ-Fe_2O_3); magnetite known to possess superior magnetic properties making it more preferable for drug delivery and tissue engineering based applications [13]. Specific applications of magnetic nanoparticles are described in the following sections and illustrated in Figure 2.2.

Magnetic nanoparticles as drug delivery carriers: The use of magnetic nanoparticles (MNPs) as drug carriers for cancer treatment is desirable as the MNPs can be attracted to the site of interest using an external magnetic field [25, 27]. But these magnetic nanoparticles do not have a bulk core, which can be loaded with a large amount of the drug and release the drug in a controlled manner over a period of time. Thus the drug can only be conjugated on the surface of magnetic nanoparticles by covalent or cleavable linkages. This leads to incorporation of only a small amount of drugs into the MNPs for targeted drug delivery. Magnetic targeting properties of the MNPs can be used as chemotherapeutic drug carriers by coating MNPs with biocompatible polymers, which can be loaded with an adequate amount of drugs to overcome this limitation [12]. Many researchers have investigated magnetic-based polymeric (core-shell) nanoparticles and established these particles for use as targeted and controlled drug delivery vehicles [24, 25, 28-32]. The targeting mechanism efficiency can be further enhanced by conjugation of targeting ligands on the surface of nanoparticles.

Magnetic nanoparticles for Magnetic Resonance Imaging (MRI): Of the variety of imaging modalities available for non invasive visualization of diseased tissues and their molecular processes, magnetic resonance imaging (MRI) has the advantages of high spatial resolution and detailed imaging of the anatomical structure of the organs and/or tissues of interest [33, 34]. Magnetic nanoparticles, especially superparamagnetic naoparticles (SPIONS) can be used as diagnostic probes for real time tracking of tumors. Also, the SPIONS possess higher sensitivity for cellular and molecular imaging allowing them to be used in lower doses [33]. Targeted SPIONs (i.e the SPIONs conjugated with targeting ligands like antibodies, peptides, dendrimers, and oligonucleotides) have a property of imaging the targeted tissues only, but not the non-

specific tissues [12]. Not only the bare SPIONs but also polymer-coated SPIONs with different kinds of core-shell nanoparticles have also been investigated as contrast agents for MRI. Along with cellular and molecular imaging, target specificity, the pharmacological effect of the drug carriers/nanoparticles and the therapeutic efficiency of the drug delivery systems can also be investigated in real time by MRI using these polymer-coated SPIONS [22].

Magnetic nanoparticles for hyperthermia: Hyperthermia refers to heating of the local tumors at 42-45ºC by using an external source of energy such as ultrasound, microwave, or laser sources [13, 35]. Magnetic nanoparticles can also be employed as agents for inducing hyperthermia. Since the application of an alternating external magnetic field reorients the magnetic nanoparticles and dissipates heat locally, which destroys the important proteins of the cancer cells, partially dissolves the cell membrane, and kills the cancerous cells at the heated area [13, 36]. Many types of magnetic nanoparticles can be used for hyperthermia treatments like ferromagnetic, ferrimagnetic and superparamagnetic nanoparticles. The ferro- and ferri-magnetic nanoparticles are permanently magnetized, which can be used to generate heat using external sources of energy, but they have a major limitation in terms of aggregation. This aggregation renders them unsuitable for drug delivery-based targeting applications in combination with hyperthermia. On the other hand, superparamagnetic nanoparticles have a tendency of magnetic attraction only in the presence of an external magnetic field and thereby consisting of less aggregation and making them best suitable agents for hyperthermia and drug delivery applications. The generation of heat inside the cancer cells caused by magnetic nanoparticles which have uptaken by the cancer cells causes selective death of the cancer cells while minimally effecting the healthy cells [37].

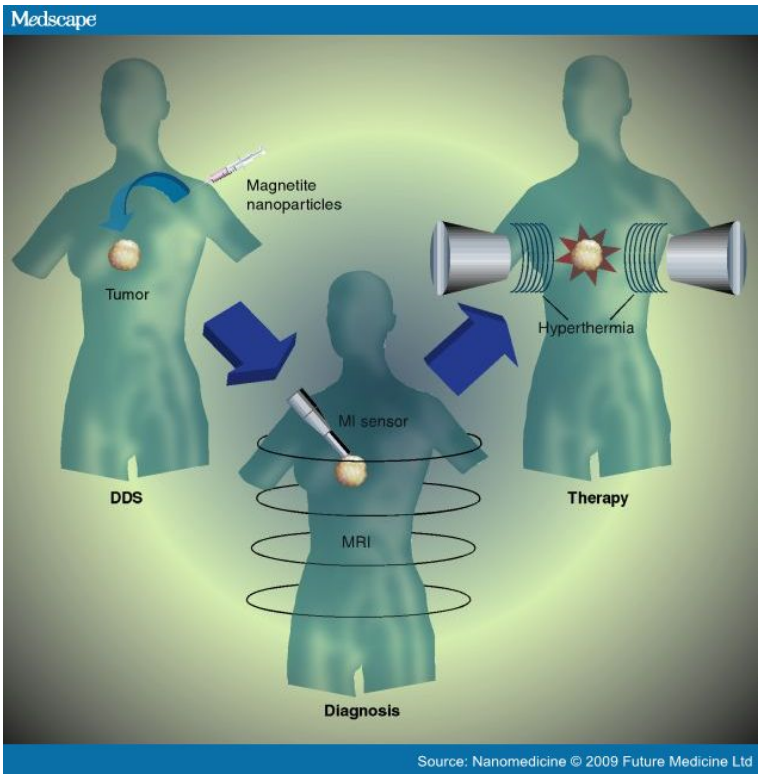

Figure 1.2 Applications of magnetic nanoparticles in drug delivery systems: hyperthermia therapy and diagnosis using MRI for cancer treatment [38].

1.2.4 Stimuli responsive nanoparticles for cancer treatment

Apart from biodegradable polymers, stimuli responsive polymers are another class of materials, which are extremely important in the synthesis of nanoparticles for drug delivery applications for cancer treatments. Different polymers have a tendency to respond to different physiological parameters like temperature, pH, ionic strength, and ligand specificity, which makes these polymers well-suited for specific drug delivery applications [19]. The intrinsic properties of these polymers to modify their physical and/or chemical properties according to the physiological conditions can be used to deliver the loaded drug by change in the stimuli [39].

Thermo-responsive polymers are a class of stimuli-responsive polymers, which respond to the change in temperature by altering their structure. The most widely known temperature-sensitive polymers for drug delivery based applications are Poly(N-isopropylacrylamide) (PNIPAAm), Polyethylene Oxide (PEO), Poly(*p*-phenylene oxide) (PPO) and Poly(Lactic acid)

(PLA). The PNIPAAm based polymers have received a lot of attention recently because they possess an LCST property near the normal body temperature, and the LCST of these polymers can be changed by co-polymerizing with either hydrophilic or hydrophobic monomers [40-42]. The PNIPAAm-based polymers have a tendency to remain hydrophilic and swollen below its LCST and collapse and become hydrophobic above the LCST thus exhibiting a unique phase transition property which can be useful for controlled drug release applications.

1.2.5 Targeting strategies for cancer

There are two mechanisms which have been explored for tumor targeting of drug-loaded nanoparticles till date. The first mechanism is the passive targeting mechanism, which does not require any modification of the nanoparticles but in fact takes advantage of the tumor's leaky vasculature and microenvironment. It is a well known that rapid tumor growth requires a continuous supply of nutrients and oxygen, leading to the formation of new blood vessels that have leaky, defective, and fenestrated vasculature. Nanoparticles carrying anticancer drugs can easily penetrate into tumors by extravasating the leaky vasculature by the Enhanced Permeation and Retention (EPR) effect. The short coming of the passive targeting strategy is are that the mechanism is not very selective of cancer cells, though it is effective for localized application of nanoparticles on the tumor site only [18].

Unlike passive targeting, active targeting is very selective to cancer cells only as it takes the advantage of over-expression of certain antigens on the surface of the cancerous cells. These over-expressed antigens are identified by proteomic and genomic methods [17]. Specific biomolecules like antibodies, proteins, peptides, and aptamers have been developed to specifically bind to the antigens presented on the surface of cancerous cells. These bioactive molecules are used to tag the nanoparticles loaded with drugs to increase the cancer cell targeting efficiency. This active targeting is called receptor-mediated targeting. Another type of active targeting is use of an external magnetic field to target the magnetic nanoparticles to the tumor site. When magnetic nanoparticles as drug carriers are guided by an external magnetic field for targeting of chemotherapeutic reagents to interested regions (tumor) only, this

mechanism is called magnetic-drug targeting. It has been shown previously that along with EPR retention of the nanoparticles at the cancer site, active targeting mechanisms have a synergistic effect on the nanoparticle accumulation in the tumor making the treatment and tracking of tumors more effective [25].

1.3 Overview of research project

The objective of this project is to develop magnetic-based core-shell nanoparticles (MBCS NPs) for targeted and controlled drug delivery applications to treat melanoma skin cancer. Towards the fulfillment of this goal, two specific aims were followed.

1.3.1 Specific aims

Aim 1: To design, synthesize, and characterize magnetic-based core-shell nanoparticles for melanoma skin cancer treatment

Aim 2: To evaluate the biocompatibility and efficiency of the system *in vitro* using various cell cultures and to assess biodistribution of these nanoparticles via preliminary *in vivo* animal (mice) models.

1.3.2 Innovative aspects of the designed system

One of the most important limitations of current chemotherapy is the development of MDR effect against anti-cancer drugs by the cancer cells after a prolonged treatment [3, 14, 19]. The MDR effect can be minimized by targeted and controlled delivery of a combination of anti-cancer drugs into the cancer cells [14, 19]. One novel aspect of this project is the development of core-shell structure and the ability to load and release two different drugs at controlled rates that could decrease the possibility of developing MDR effect. Inclusion of functionalized magnetic nanoparticles into the core-shell nanoparticles makes the particles suitable for magnetic drug targeting, MRI imaging, and hyperthermia treatments. The modification of the nanoparticle with synthetic peptide GRGDS is expected to make the system more efficient by dual targeting approach; magnetic- and receptor-mediated targeting.

1.3.3 Successful outcomes of the project

The successful outcome of this project would provide a deeper insight into the effectiveness of combined chemotherapies and targeting mechanisms for cancer treatment. Also immediate and prolonged treatment using dual drug release capability at different controlled rates is expected to be more efficient treatment method. Ultimately, monitoring tumor growth simultaneously with treatment by MRI will provide a real-time theranostic application of the nanoparticles.

CHAPTER 2

SYNTHESIS AND *IN VITRO* CHARACTERIZATION OF MAGNETIC-BASED CORE-SHELL NANOPARTICLES

2.1 Introduction

Application of nanotechnology to cancer therapeutics and diagnosis has received a lot of attention recently due to several favorable characteristics of different types of nanoparticles incorporated with drugs and imaging agents for simultaneous controlled drug delivery and tracking of cancerous tissues [12, 43, 44]. For these purposes, many researchers have developed core-shell nanoparticles using a combination of biodegradable synthetic polymers, natural polymers, stimuli responsive polymers, magnetic nanoparticles, and so on. These approaches allow integrating many desirable features into a single nanoparticle [25, 40, 44]. On the similar lines, our research aims at the establishment of multifunctional nanoparticles loaded with two chemotherapeutic drugs with one drug in the biodegradable polymer core incorporated with magnetic nanoparticles and the other one in the thermo-sensitive polymer shell of the nanoparticles, making the nanoparticles suitable for controlled and targeted combination chemotherapy, hyperthermia treatment, and real-time MR imaging of tumors. In this chapter, we demonstrate the formulation and characterization of these magnetic-based core-shell nanoparticles.

2.2 Materials and Methods

2.2.1 Materials

Poly (D, L lactide-co-glycolide) (PLGA, 50/50 with carboxyl end groups, Lakeshore Biomaterials), Magnetite nanoparticles (Meliorum technologies), Dichloromethane (DCM, MERCK KGaA), Doxorubicin (Tocris Bioscience) and foamvar coated-copper TEM grids (Electron

microscopy sciences) were purchased as used as obtained. The chemicals, Poly (vinyl alcohol) (PVA, 87-89%) Curcumin, N-Isopropylacrylamide (NIPAAm, 97%), Sodium dodecyl sulfate (SDS, 99%), N,N-Methylenebisacrylamide (BIS), Potassium persulfate (KPS, 99+%), Vinyltrimethoxysilane (VTMS, 98%), iron assay kit, ethanol (95%), acetic acid, TEMED, Acrylamide and Allylamine were purchased from Sigma-Aldrich. Dulbecco's Modified Eagle's Medium (DMEM), Neonatal calf Serum (NCS), penicillin-streptomycin, and 1X trypsin EDTA were purchased from Invitrogen (Carlsbad, CA).

2.2.2 Formulation of MBCS NPs

The MBCS NPs were developed by a layer by layer synthesis process. The core of the nanoparticles consisted of biodegradable polymer PLGA and functionalized magnetite nanoparticles along with hydrophobic model drug curcumin. The shell of the nanoparticles consisted of the thermosensitive polymer (PNIPAAm-AAm-AH) loaded with hydrophilic anticancer drug Doxorubicin as shown in Figure 3. The Poly (D, L lactide-co-glycolide)-magnetite (PLGA-MNPs) core of the particles was formulated by an oil/water (O/W) emulsion process as mentioned in previous studies [24, 28, 29, 31]. The PLGA-MNPs core was further functionalized with Allylamine by EDC/NHS chemistry [32], and monomers of NIPAAm, AAm, and AH were copolymerized on the nanoparticles by a free radical polymerization to develop a thermosensitive shell on the functionalized PLGA-MNPs core as previously described [40, 45]. The amount of magnetite nanoparticles (%w/w) that were successfully encapsulated into the MBCS NPs was determined by iron assays. In order to increase the magnetite encapsulation efficiency, the magnetite nanoparticles were chemically functionalized using VTMS and these functionalized magnetic nanoparticles were used to synthesize the MBCS NPs using the same step by step formulation procedures. The iron assay on MBCS NPs encapsulated with modified magnetite nanoparticles showed a significant increase in the iron content as compared to those of encapsulation with bare magnetite nanoparticles. Thus for all the further studies, functionalized magnetite nanoparticles were used for MBCS NP synthesis.

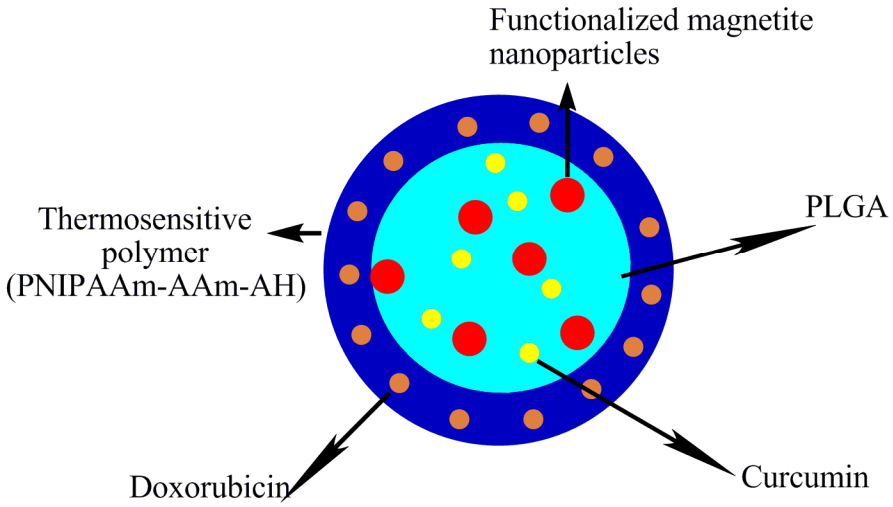

Figure 2.1 Design of the MBCS NPs

2.2.3 Coupling of the magnetite nanoparticles with a silane coupling agent VTMS

Iron oxide nanoparticles were functionalized with VTMS as mentioned in our previous studies by acid catalyst hydrolysis and electrophilic substitution of Fe_3O_4 nanoparticles; illustrated in Figure 2.2(A) [40]. Briefly, iron oxide nanoparticles (0.074214 g) were suspended in 99% (v/v) ethanol solution in Deionized (DI) water and sonicated for 20 minutes at 10W (Misonix Inc., 3000, Farmingdale, NY). 3 ml of Acetic acid (CH_3COOH) was then added to the MNP dispersion and again sonicated the solution under same conditions for 10 more minutes. The solution was then transferred to a plastic beaker, which was kept stirring on a magnetic stir plate at 400-500 rpm. 0.49 ml of VTMS was added to the nanoparticle solution, and the beaker was sealed tightly to prevent evaporation of ethanol during the reaction time of 24 hours. At the end of the reaction time, the nanoparticles were collected using an external magnet and washed extensively with 99% (v/v) ethanol solution in DI water before further use.

2.2.4 Synthesis of the PLGA-Magnetic nanoparticles

PLGA-MNP nanoparticles were synthesized by an O/W emulsion technique as shown in Figure 2.2(B). Briefly 100 mg of PLGA (50:50) was dissolved in 5 ml of DCM. 10 mg of previously synthesized silane coupled iron oxide nanoparticles were added to the PLGA-curcumin solution

and sonicated using an ultrasonicator at 30 W for 15 minutes to allow dispersion of the functionalized magnetic particles in DCM. The resulting dispersion was quickly added in a dropwise manner to 2% (w/v) PVA solution, which was kept stirring on a magnetic stirring plate. After the oil phase was added to the water phase, the resulting solution was emulsified by sonication at 20 W for 2 minutes. The emulsified solution was then kept stirring again on the magnetic stir plate for 6 hours to allow evaporation of DCM and formation of stable PLGA-MNP nanoparticles. After 6 hours, the resulting nanoparticle solution was centrifuged at low speed; 1000 rpm for 2 minutes to allow separation of unencapsulated magnetic nanoparticles from PLGA-MNPsi nanoparticles. The supernatant was collected and centrifuged at 20,000 rpm (Beckman Coulter, Inc., Fullerton, CA) for 20 minutes. The supernatant containing unloaded drugs was collected and the resulting nanoparticle pellet was resuspended in DI water, and followed by lyophilization to collect the nanoparticles for further use.

2.2.5 Functionalizing surfaces of PLGA-Magnetic nanoparticles

In order to modify the carboxyl (COOH) functional group presented on the PLGA-MNP core to facilitate conjugation of thermosensitive polymeric shell on the top, EDC/NHS binding method was used as shown in the reaction scheme of Figure 2.2(C). Briefly, 20 mg of PLGA MNPs were dispersed by sonication at 30 W into 30 ml of 0.1 M MES buffer (pH 4.8-5.2) for 10 minutes. The solution was transferred onto the magnetic stirring plate, and 100 mg of EDC and 100 mg of NHS was added to the nanoparticle solution. Further, 130 µl of Allylamine was added to the solution. Finally, 14 mg of Sodium Dodecyl Sulphate (SDS) was added to the solution, and the reaction was continued for 4-6 hours. At the end of the reaction, the solution was centrifuged using ultracentrifuge at 20,000 rpm for 20 minutes. The obtained nanoparticle pellet was resuspended in DI water and lyophilized before further use.

2.2.6 Copolymerizing NIPAAm, AAm and AH onto the amine-functionalized PLGA-Magnetic nanoparticles

The functionalized PLGA-MNP nanoparticles were used as a template to copolymerize NIPA, AAm, and AH on the top of the particles by a free radical polymerization technique as

shown in Figure 2.2(D). Briefly, 0.028 gms of PLGA-MNP-AH nanoparticles, 0.0581 gms of NIPA, 0.011 gms of Am, and 0.0131 gms of BIS was added to 100 ml DI water; and the solution was sonicated for 2 minutes at 20 W to allow dispersion of the nanoparticles. SDS (0.03g) was added as a surfactant to stabilize the nanoparticles, and the suspension was sonicated for 1 minute at 20 W. The solution was tranferred to a conical beaker on a magnetic stir plate and purged with Argon gas for 30 minutes to allow creation of an inert atmosphere and removal of oxygen from the flask. Initiatior APS (0.080 g), accelarator TEMED (10 µl), and AH (70 µl) was added in a beaker while the inert atmosphere was maintained. The reaction was continued for 4-6 hours under the inert atmosphere and at the end of the reaction, the particles were collected by centrifugation at 20,000 rpm for 20 minutes.

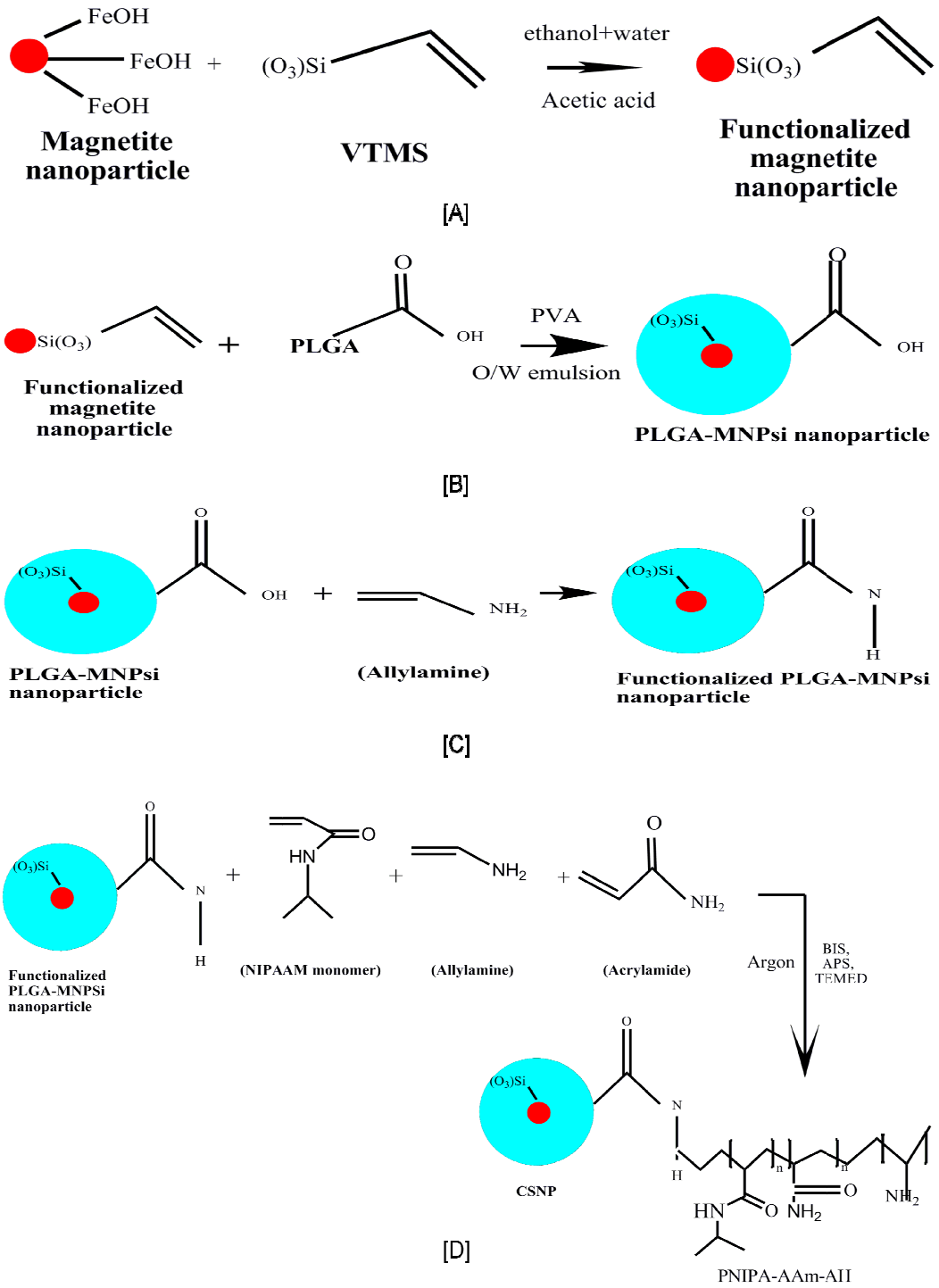

Figure 2.2 [A] Synthesis procedure of VTMS functionalized magnetite nanoparticles, [B] Synthesis of PLGA-MNPsi nanoparticles, [C] Functionalizing PLGA-MNPsi nanoparticles with Allylamine, [D] Coating of thermosensitive polymer PNIPA-AAm-AH on the functionalized PLGA-MNPsi nanoparticles

2.3 Characterization of the nanoparticles

2.3.1 Iron assays for comparison of the amount of bare magnetite Vs functionalized magnetite encapsulated into MBCS NPs

Measurement of the iron content % (w/w) in MBCS NPs prepared using either non-functionalized magnetic nanoparticles or silane-functionalized nanoparticles was done by iron assay techniques as described earlier [36]. Sample nanoparticles from both the batches were suspended into DI water to make particle suspensions and analyzed for the iron content. The standards were made from original magnetic nanoparticles suspended into DI water in a series of known concentrations. All the samples and standards were added to a 48- well plate. 100µL of 30% (v/v) HCL solution was added to all the samples and standards for two hours at 55˚C to dissolve the iron oxide. After two hours of incubation, 100µL of 1mg/ml Ammonium per sulphate (APS) solution was added to all the samples and standards and incubated again for 15 minutes. 100 µL of 0.1M potassium thiocyanate (PTC) was then added to all samples and standards and again incubated for 15 minutes. At the end of this process, the amount of iron oxide in the nanoparticles from both batches was calculated by comparison with the standards using UV-Vis spectroscopic measurements (Infinite M200 plate reader, Tecan), following the manufacturer's instructions at 428 nm wavelength [46].

2.3.2 Transmission electron microscopy (TEM), Dynamic light scattering (DLS), and zeta potential measurement

Lyophilized MBCS NPs were suspended in Phosphate Buffer Saline (PBS), sonicated at 20 W till dispersed. 10 µl of nanoparticle solution was added on a Foamvar coated copper grid (Biosciences). The nanoparticles were allowed to settle down and dry on the grid before analyzing the sample in TEM (Technai) instrument.

Nanoparticle samples from each synthesis step where resuspended into DI water to make a final concentration of 0.5 mg/ml. In each vial 2 ml of the suspension was taken and analyzed for nanoparticle size, polydispersity and surface charge by Zeta potential analyzer (Brookhaven Instruments, Holtsville, NY).

2.3.3 Fourier Transform Infrared Spectroscopy (FTIR)

After each step of nanoparticle synthesis, the sample of nanoparticles was collected, lyophilized, and then 1 mg of particles was added to labeled glass vials. All the samples were prepared in DCM and added one after another on the Quartz windows used for FTIR analysis (Nicolet 6700 FT-IR spectrometer, Thermo Fisher Scientific).

2.3.4 Magnetic property measurement

The superconducting quantum interference device magnetometer (Quantum design) was used to determine the magnetic property of the MBCS NPs as compared to the bare MNPs. The same concentrations of iron oxide in control magnetite nanoparticles as well as MBCS NPs sample were weighed and embedded into epoxy resin capsules. The room temperature analysis of the magnetic property was done by varying the magnetic field, and the coercivity and remenance values were determined from the hysteresis loop.

2.3.5 Lower critical solution temperature (LCST) measurement of the PNIPAAm-AAm-AH thermosensitive polymer by UV/Vis spectroscopy

Thermosensitive (PNIPAAm-AAm-AH) tripolymer nanoparticles were synthesized as mentioned in section 2.2.5 but without using the functionalized PLGA-MNP core. The LCST was determined using a UV/Vis spectrophotometer coupled with a temperature controller. PNIPAAm-AAm-AH nanoparticle (3% w/v) suspension in DI was made and heated from 25˚C to 41˚C and analyzed in the spectrophotometer at 500 nm wavelength at each 2˚C interval. The obtained absorbance values were converted to % transmittance and plotted against the corresponding temperature to obtain the LCST value of the polymer (Temperature at 50% transmittance, where the absorbance changed from high to low).

2.3.6 Ligand conjugation efficiency of the MBCS NPs

To check the ligand binding efficiency of our nanoparticles for future bioconjugation using peptides, MBCS NPs (10 mg) were suspended into 0.5 mL of 0.1M MES buffer (pH 4.8-5.2). The

nanoparticle suspension was activated by adding 0.01 mg of EDC and 0.01 mg of NHS, and the reaction was carried out for 10 minutes at room temperature. Fluoro-PEG-SCM (0.2 mg) was added to the solution, and the reaction was continued for 24 hours on a mechanical shaker under dark conditions. At the end of the reaction, the suspension was ultracentrifuged at 20,000 rpm for 20 minutes, and the supernatant was discarded. The nanoparticles were thoroughly washed with DI water, suspended into 50% glycerol and imaged under Zeiss cytoviva fluorescent microscope.

2.3.7 Drug loading and release study from the MBCS NPs

For drug loading and release studies, two types of drugs: hydrophobic drugs, (e.g. curcumin), and hydrophilic drugs, (e.g. doxorubicin) were used. Curcumin is a polyphenolic compound, which is known to possess anti-angiogenic properties and inhibitory effects on organ metastatis caused by melanoma [14, 47]. Thus curcumin was chosen as a model anti-cancer drug to be used for our melanoma therapy. Curcumin (30 mg) was loaded into the core of the MBCS NPs along with functionalized magnetic nanoparticles during the O/W emulsion process mentioned in section 2.2.3, and the same synthesis procedures were carried out as mentioned in sections 2.2.4 and 2.2.5. The curcumin loading efficiency was calculated by an indirect method using the following formula.

$$\text{Percentage loading efficiency} = \frac{\text{amount of drugs used} - \text{amount of drugs in supernatant}}{\text{amount of drugs used}} \text{ x } 100\ \%$$

For curcumin release studies, the curcumin-loaded MBCS NPs were suspended in a concentrated (1 mg MBCS NPs/ 1 ml 50% (v/v) ethanol solution). In each drug release tube, 1 ml of nanoparticle suspension was added, and the samples were placed at designated temperatures (n=3). At each time point, the tubes were centrifuged at 12,000 rpm for 15 minutes and 0.5 ml of the supernatant was collected and 0.5 ml of 50% (v/v) ethanol solution was added to all the samples. The drug release study was carried out for a period of 25 days, and the samples were analyzed using UV/Vis spectrophotometer at 428 nm. The drug release study was done at two temperatures; 25˚C (below LCST of the thermosensitive shell) and 41˚C (above LCST of the

thermosensitive shell) to analyze the effect of the LCST behavior of the polymeric shell on the curcumin release from the core.

Besides curcumin, doxorubicin was also used in drug loading and release study. Doxorubicin, a potent anti-cancer agent against several forms of cancers like thyroid, breast, stomach, and lungs, has also exhibited significant anti-cancer effects against melanoma tumor growth and metastasis [48], making it a suitable choice for our drug delivery system. Freeze dried MBCS NPs (10 mg) were suspended into 10 ml (0.02% w/v) doxorubicin-HCL solution. The suspension was kept stirring at 4˚C for 3 days to allow drugs loaded into the thermosensitive polymeric shell of the MBCS NPs. After 3 days, the MBCS NPs were ultracentrifuged, and the supernatant containing the unloaded drug was collected for determination of the doxorubicin loading efficiency.

For doxorubicin release studies, the nanoparticles were resuspended in 10 ml PBS, and 1 ml of nanoparticle suspension was added in each drug release tube. The samples were placed at designated temperatures (n=3). At each time point, the tubes were centrifuged at 12,000 rpm for 15 minutes, 0.5 ml of the supernatant was collected and 0.5 ml of PBS was added to all the samples. The drug release study was carried out for a period of 7 days and the samples were analyzed at an excitation wavelength (λex) of 470 nm and an emission wavelength (λem) of 585 nm using UV/Vis spectrophotometer.

2.3.8 Human Dermal Fibroblasts (HDFs) and Murine Melanoma (B16F10) cell culture

Human dermal Fibroblast cells (HDF) and Melanoma cells (Murine, B16F10) were cultured in complete Dulbecco's Modified Eagle Medium (DMEM) supplemented with 10% serum and 1% penicillin-streptomycin and maintained at 37˚C, 5% CO_2 in humid atmosphere of an incubator. Upon reaching 80-90% confluency, cells were passaged, and for all experiments cells up to passage 10 were used.

2.3.9 Pharmacokinetic study by B16F10 viability assessment

Treatment efficiency of our MBCS NPs loaded with drugs was compared to the activities of free drugs. B16F10 cells were cultured as mentioned in section 2.3.8. The cells were exposed to different groups like free curcumin, free doxorubicin, combinations of curcumin and doxorubicin in known concentrations of drugs (0, 1, 5, 10, 25, and 50 μg/ml) for a period of 24 hours. In comparison to these groups, MBCS NPs loaded with curcumin, doxorubicin and a combination of curcumin and doxorubicin as mentioned in section 2.3.7 were also exposed to the B16F10 cells using the same drug concentrations calculated from loading efficiency values. For MBCS NPs loaded with Doxorubicin, the effect of temperature was also analyzed at 37˚C and 41˚C. The cells were incubated with samples for a period of 24 hours after which they were analyzed by MTS assays as mentioned in section 2.3.9.

2.3.10 HDF Cell viability study

Interactions of the MBCS NPs with HDFs were evaluated using MTS assays. HDFs were cultured as mentioned in section 2.3.8, seeded at a density of 5000 cells/well in a 96-well plate and allowed to attach overnight. Nanoparticle suspensions in various known concentrations (0, 10, 50, 100, 200, 300, and 500 μg/mL) were added to the cells and incubated at 37˚C, 5% CO_2 for 24 hours. At the end of the incubation time, the nanoparticle suspensions were removed, and the cells were supplemented with complete DMEM media to which 20 μL of MTS reagent was added. The cells were incubated with the MTS reagent for 2 hours, and then spectrophotometer measurements were taken at 540 nm to determine cell survival. Cells exposed to complete media without any nanoparticles served as control samples.

2.3.11 Iron assays for quantification of uptake of MBCS NPs by B16F10 (Murine Melanoma cells)

In order to investigate the cellular uptake efficiency of MBCS NPs by B16F10 cells, the cells were seeded in 48 well-plates at a density of 10,000 cells/well and allowed to grow for 24-hours at 37˚C. The MBCS NPs solutions of known concentrations were prepared in complete

DMEM media (0, 10, 50, 100, 200, 300, and 500 µg/mL) and added to the cells for an incubation time of 6 hours. After incubation time, the nanoparticle media solution was removed and the cells were washed 3-4 times with PBS. The cells were incubated with 1% Triton in PBS for one hour to allow the cells to be lysed.

The cell lysis solutions were analyzed by iron assays for the presence of iron content in the cell lysis samples. Briefly, 100 µl cell lysate was incubated with 30% v/v HCL solution at 55℃ for 2 hours, and then 100 µl (1 mg/ml) of APS solution was added to all the samples for 15 minutes. Then after, 100 µl of (0.1M) potassium thiocyanate solution is added to all the samples for 15 more minutes of incubation and the aborbance of each sample was read at 478 nm using UV-Vis spectrophotometer. The remaining cell lysate was analyzed for total DNA content using a Picogreen DNA assay (Invitrogen Corporation, California) following manufacturer's instructions. The iron content resulted from the iron assay was normalized by the amount of DNA presented per sample.

2.3.12 MBCS NP's uptake visualization by Prussian blue staining

The uptake study of MBCS NPs was performed as mentioned above. At the end of incubation time, the cells were washed with PBS several times and then fixed with 2% glutraldehyde solution at room temperature for 20 minutes. After fixation, the cell membranes were permeabilized using 0.1% triton in PBS for 5 minutes at room temperature. The triton was removed at the end of 5 minutes and the cells were washed with PBS. To stain the iron oxide presented in the MBCS NPs uptaken by the cells, 50:50 potassium ferrocyanide and hydrochloric acid solution was added to the cells for 20 minutes. The iron staining solution was then removed, and the cells were rinsed with PBS. The diluted pararosaniline solution was added to stain the cell membrane and the chromatin material pink. The cells incubated without nanoparticles and stained using the same method were used as control. The cells were visualized under the microscope and imaged using Axio Vision Software.

2.3.13 Use of MBCS NPs as contrast agents for MRI *in vitro*

For preparation of agarose phantoms, 0.5% (w/v) agarose solution in water was kept boiling at 100˚C till the solution turned completely transparent. The solution was allowed to cool down to room temperature and then MBCS NPs were added to the agarose solution to make samples of known concentrations (0.33 mg/ml and 0.66 mg/ml). The samples were immediately transferred to 4˚C to allow gelation of agarose and saved at same conditions till further use.

B16F10 murine melanoma cells were cultured as described earlier and grown till confluency. The cells were trypsinized, counted and plated at a density of 10^6 cells in a T75 cell culture flask. The cells were allowed to attach overnight and MBCS NPs in a known concentration (300µg/ml) were added to the cells and incubated for 2 hours to allow the MBCS NPs to be uptaken by the cells. The media was then removed and the cells were gently rinsed 5 times with PBS. After removal of PBS the cells were trypsinized, centrifuged and the cell pellet was suspended into a prepared agarose solution at room temperature. The agarose solution was gelled at 4˚C. The agarose phantoms, containing 10^6 B16F10 cells only and cells which were incubated with PLGA nanoparticles (300µg/ml), were used as controls. The samples and control phantoms were imaged using 4.7T Varian small animal MRI scanner as described elsewhere [40].

2.3.14 Statistical Analysis

Results obtained were analyzed using one way ANOVA with $p < 0.05$ and Bonferroni Post-hoc tests (GraphPad Prism version 5.02 for Windows) All the results are presented as mean ± SD.

2.4 Results and Discussion

2.4.1 Comparison of the amount of bare magnetite Vs functionalized magnetite nanoparticles encapsulated into MBCS NPs

The amount of magnetite encapsulated into the MBCS NPs using either bare magnetite nanoparticles or silane-coupled magnetite nanoparticles was done by iron assays. As illustrated

in Figure 2.3, the amount of magnetite encapsulated was 3.22% (w/w) when bare MNPs were used, whereas the amount of VTMS-coupled magnetite to be encapsulated into the same amount of MBCS NPs, was 16.33% (w/w). It has been well illustrated previously in many other researches that the MNPs without any coating have hydrophobic surfaces with a very high tendency to aggregate. Functionalization of MNPs with thiols, silica, oleic acid, and others make the MNPs redispersible and stable in aqueous solutions easily, leading to a higher amount of encapsulated particles [13]. The speculated reason for better encapsulation of the silane-coupled magnetite nanoparticles into the MBCS NPs is thus due to better dispersion, less aggregation of the functionalized magnetite nanoparticles, and more presence of thiol groups on the magnetite nanoparticles, which results in better interactions with the polymer as previously reported [11, 49].

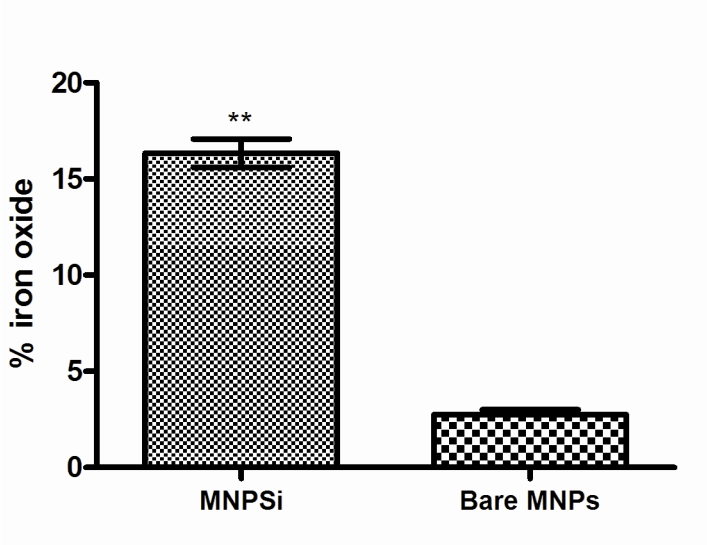

Figure 2.3 Amount of magnetite nanoparticles encapsulated into MBCS NPs in %w/w; * indicates significance compared to other samples, $p<0.05$ (n=3)

2.4.2 Core-shell structure, morphology, size, and surface charge of the nanoparticles

To determine the shape, size and the core-shell structure, TEM images of the nanoparticles were taken. As shown in the Figure 2.4, the MBCS NPs were 300-350 nm in size. The presence of the magnetite nanoparticles throughout the PLGA core was evident in the inset

figure. The presence of PNIPAAm-AAm-AH tripolymer shell surrounding the particles was also seen clearly in the inserted image.

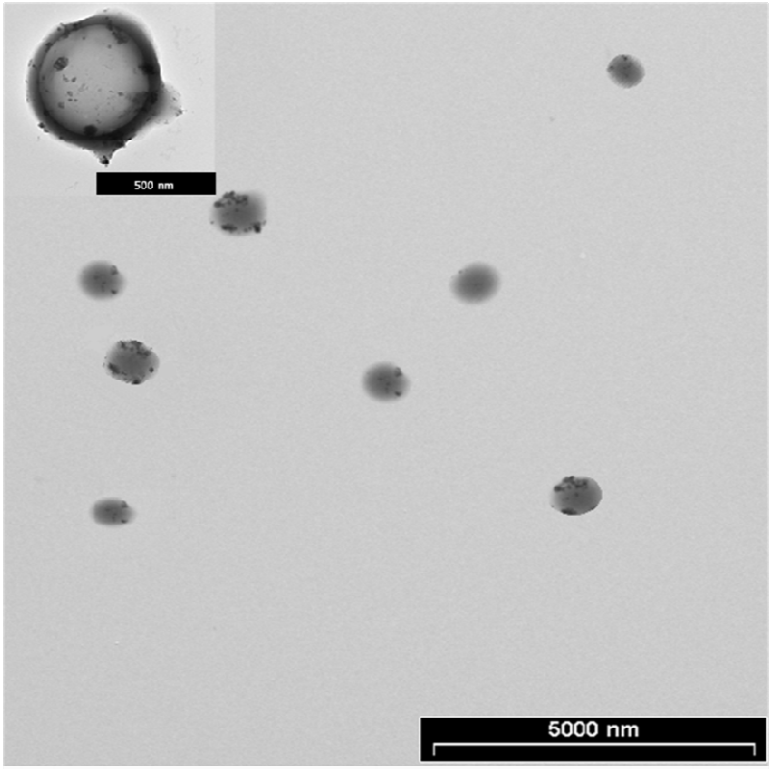

Figure 2.4 TEM image of the MBCS NPs; inset shows the core shell structure of the nanoparticles of 300-350 nm in size.

At each step of core-shell nanoparticle synthesis, the hydrodynamic size, the polydispersity index, and zeta potential of the particles were measured by DLS technique. The results are illustrated in Table 2-1. The mean hydrodynamic diameter of the final core-shell nanoparticles (MBCS NPs) is 299 ± 15.2 nm with the polydispersity index of 0.278 ± 0.018 and the zeta potential of -12.07 ± 0.18 mV, thus indicating that the final nanoparticles are stable.

Table 2.1 Hydrodynamic sizes, respective polydispersities, and surface charges (Zeta Potential) of nanoparticle samples

Sample	Size (nm)	Poly dispersity	Zeta potential (mV)
PLGA-MNPSi core nanoparticles	233.9 ± 4.10	0.112 ± 0.053	-16.46 ± 0.45
Allylamine functionalized PLGA-MNPSi nanoparticles	256.6 ± 1.70	0.112 ± 0.023	-10.09 ± 0.30
MBCS NPs (PLGA-MNPSi-AH-tripolymer nanoparticles)	296.0 ± 15.2	0.278 ± 0.018	-12.07 ± 0.18

2.4.3 Chemical composition of the nanoparticles

After each step of nanoparticle synthesis, the FTIR spectroscopy was done on lyophilized nanoparticles to confirm the chemical composition of the nanoparticles [50, 51]. As shown in Figure 2.5(A), the peak at 3496.2 cm^{-1} corresponds to OH stretching due to presence of carboxylic acid of PLGA-MNP particles. The sharp and intense peak at 1750 cm^{-1} is a characteristic peak of the carbonyl group of ester. Also the peaks in the range of 700-800 cm^{-1} correspond to the vinyl double bond stretching due to presence of vinyl conjugated magnetite into the PLGA nanoparticles. Figure 2.5(B) corresponds to the Allylamine-functionalized PLGA-MNPsi nanoparticles. The peaks in the range of 1550-1650 cm^{-1} represent the coupling of the C=OH bonds presented on the surface of PLGA that were interactive with Allylamine ($-NH_2$) to form an amide bond ($C=ONH_2$). The conjugation of PNIPAAm-AAm-AH onto the functionalized PLGA-MNPsi intensifies the OH stretching bond at 3500 cm^{-1} due to polymer hydration in Figure 2.5(C).

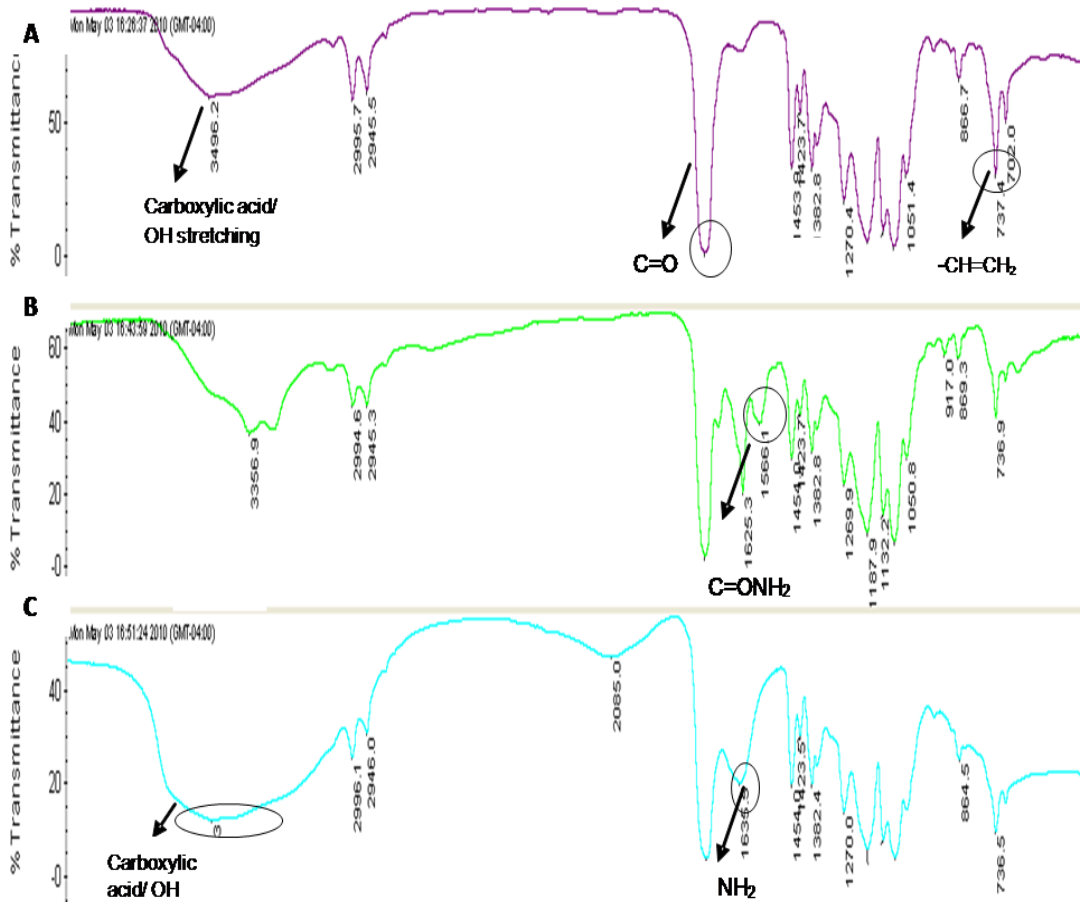

Figure 2.5 FTIR spectrum of (A) PLGA-MNPSi core nanoparticles, (B) Allylamine-functionalized PLGA-MNPSi nanoparticles, and (C) MBCS NPs (PNIPAAm-AAm-AH conjugated PLGA-MNPSi nanoparticles)

2.4.4 Magnetic properties of the MBCS NPs

To compare magnetic properties of MBCS NPs to bare magnetite nanoparticles, SQUID magnetometer was used. As shown in the Figure 2.6, the magnetic property of the MBCS NPs was reduced as compared to bare magnetite nanoparticles. This reduction might be due to the presence of the PLGA core as well as the PNIPAAm-AAm-AH tripolymer shell onto the functionalized magnetite nanoparticles,. This result was in a good agreement with previous results where the saturation magnetization was decreased due to the incorporation of polymeric layer on the magnetic nanoparticles that caused lessened magnetic attraction of the magnetic particles because of the polymeric barrier [24, 31, 52, 53]. As reported in the previous stuides,

the range of Saturation magnetization (*Ms)* applicable for drug delivery and tissue engineering based applications is 7-22 emu/g [30, 54, 55]. Thus our MBCS NPs which possess an *Ms* of 15.65 emu/g would still be suitable for magnetic drug targeting applications. The coercivity of the MBCS NPs was negligible in the absence of an external magnetic field and the remanence at low magnetic field was minimal indicating the superparamagnetic behavior of our MBCS NPs just like the bare magnetite nanoparticles as indicated in Table 2-2.

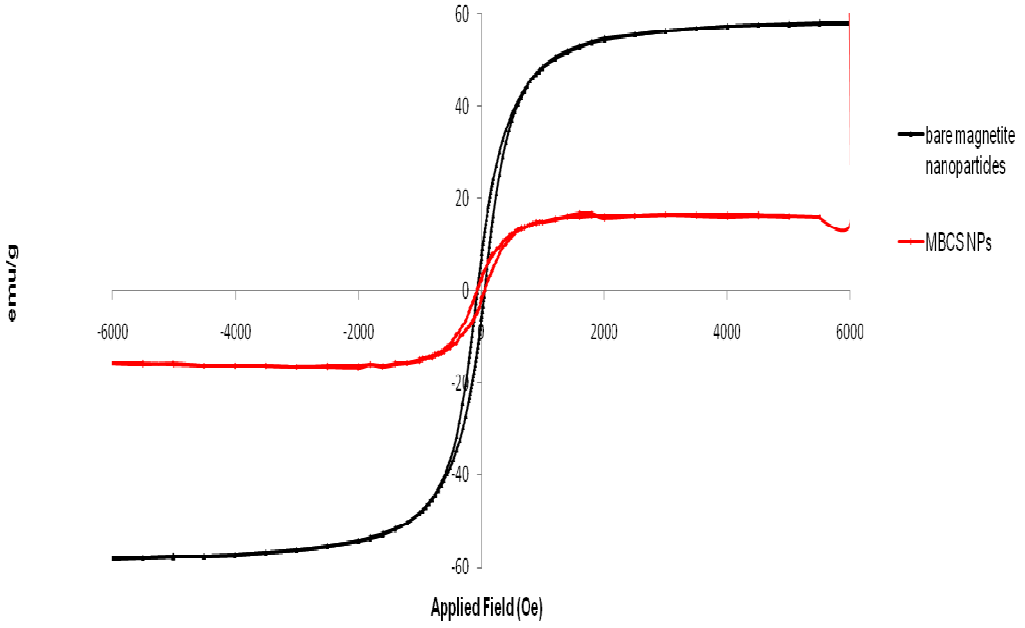

Figure 2.6 SQUID measurements for magnetic property analysis of bare magnetite nanoparticles and MBCS NPs

Table 2.2 Saturation magnetization, Remanence and Coercivity of MBCS NPs

sample	Saturation magnetization (M_s) emu/g	Saturation remanence (M_r)	Remanence(Ms/Mr)	Coercivity (H_C)
Bare magnetite	57.88	7.06	8.19	2
MBCS NPs	15.65	2.14	7.31	1

2.4.5 LCST behavior of the thermosensitive shell

The LCST of the PNIPAAm-AAm-AH thermosensitive tripolymer, which was conjugated onto the functionalized PLGA-MNPsi nanoparticles, was determined by UV/Vis spectrometry method. The phase transition in the tripolymer occurred relative to the increase in temperature. The temperature at which the transmittance of the polymer was 50% was the LCST. For the PNIPAAm-AAm-AH tripolymer, the LCST was around 39.5˚C (results not shown). This result is consistent with the findings reported earlier by our group [56].

2.4.6 Conjugation efficiency of the MBCS NPs to Fluoro-PEG-SCM

Before targeting the developed nanoparticles to melanoma tumors by incorporation of specific peptides onto nanoparticle surfaces, it was important to analyze the conjugation efficiency of the nanoparticles. For this purpose, fluorescent PEG was conjugated by EDC/NHS chemistry on the surface of MBCS NPs which possess an active amine functional group. Figure 2.7 exhibits the successful conjugation of Fluoro-PEG-SCM on the MBCS NPs which is in accordance with earlier research [56].

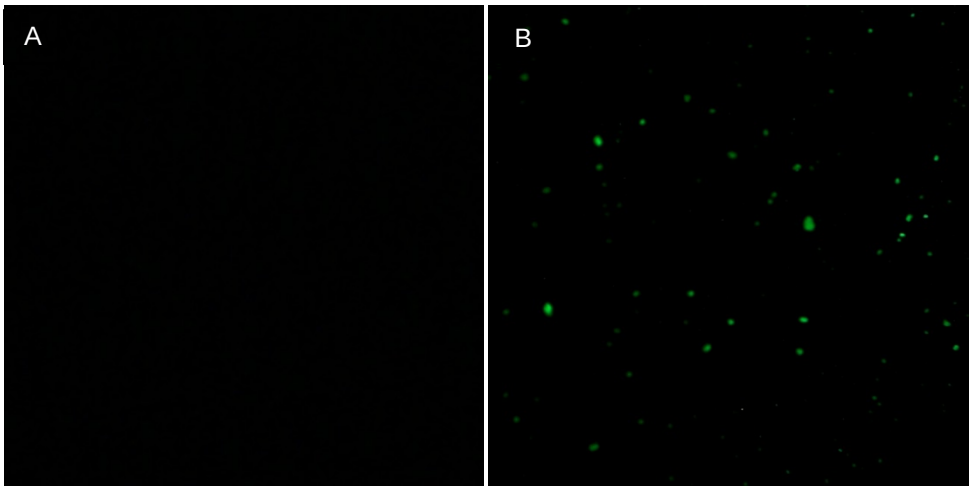

Figure 2.7 Ligand conjugation efficiency: (A) MBCS NPs without Fluoro-PEG-SCM and (B) Conjugation of MBCS NPs by Fluoro-PEG-SCM

2.4.7 Drug loading efficiency and drug release kinetics of the MBCS NPs

The loading efficiency of curcumin determined by the formula stated in the section 2.3.8 was approximately 68.30%. There was not much difference in the curcumin release at temperatures 25˚C and 42˚C indicating that the release of curcumin from PLGA was not dependent on change in temperature. There was negligible release of curcumin for the first 96 hours as expected because of the coating of the thermosensitive shell, which might hinder the release of curcumin until the beginning of bulk degradation of the PLGA-MNPSi core. This result is in accordance with previous results from our group using Multilayered microparticles [57]. The burst release of curcumin started after 72 hours and ended at 25 days as shown in Figure 2.8, about 72-78 % of the drug was released over 25 days making MBCS NPs suitable for use as drug delivery carriers for sustained drug release applications.

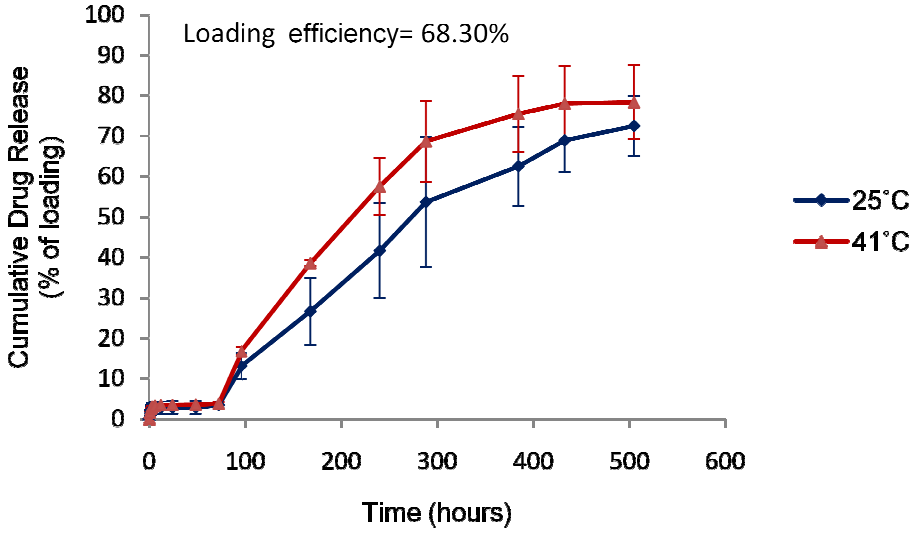

Figure 2.8 *In vitro* Curcumin release from the core of MBCS NPs at 25˚C and 41˚C temperature. Values are presented as mean ± SD (n=3).

The loading efficiency of doxorubicin from the thermosensitive polymer shell of the MBCS NPs was also calculated by using the equation in section 2.3.8 and found to be 59.32%, which was in the range of loading efficiencies found for PNIPA-based thermosensitive nanoparticles described earlier [40, 58]. As shown in the Figure 2.9, the release of doxorubicin from the

PNIPAAm-AAm-AH tripolymeric shell was significantly higher at 41˚C (above LCST) compared to 25˚C (below LCST), establishing the temperature-sensitive behavior of the polymer shell. The release at both temperatures exhibited a similar trend with burst release occurred during first 24 hours, which might be due to the presence of some doxorubicin on the surface of the nanoparticles. The period of 25 hours to 168 hours showed a sustained release of doxorubicin at both temperatures. The percent of drug released after 168 hrs at 25˚C was around 27.97%, while at 41˚C, the cumulative release was 43.88%. Thus the temperature dependent drug release characteristic of our MBCS NPs seemed to be an important characteristic for drug delivery systems requiring target specific burst release in response to changes in temperature.

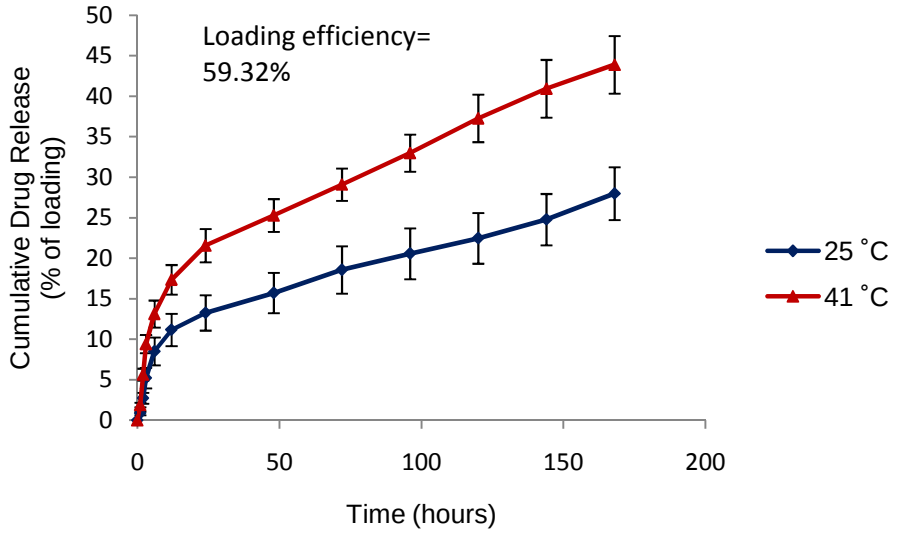

Figure 2.9 *In vitro* Doxorubicin release from the thermosensitive polymer shell of MBCS NPs at 25˚C and 41˚C temperature. Values are presented as mean ± SD (n=3).

2.4.8 Pharmacokinetic study

The effect of the model drugs curcumin, doxorubicin, and a combination of both the drugs was compared to the effect of our MBCS NPs loaded with curcumin in the core, doxorubicin in the shell and both the drugs loaded in the MBCS NPs. As illustrated in figure 2.10A, both free curcumin and MBCS NPs loaded with curcumin were toxic to the melanoma cells in a dose dependent manner. At lower doses (0-25 µg/ml), free curcumin exhibited no significant toxic

effects on the B16F10 cells. The cell viability was significantly reduced to 37% at 50 µg/ml while for the curcumin-loaded MBCS NPs, the cell viability was about 60% for concentrations of 10-50 µg/ml. Cells when exposed to doxorubicin from 1-50 µg/ml, the viability was around 20%. The cell viability was greatly reduced when the cells were exposed to MBCS NPs loaded with doxorubicin at 41˚C as compared to 37˚C. The effect of a combination of curcumin and doxorubicin on the cell viability was higher than effect of curcumin and doxorubicin. From the pharmacokinetic studies, the effect of the released drugs on the cells was evaluated which provide us with the optimum doses for future treatment studies.

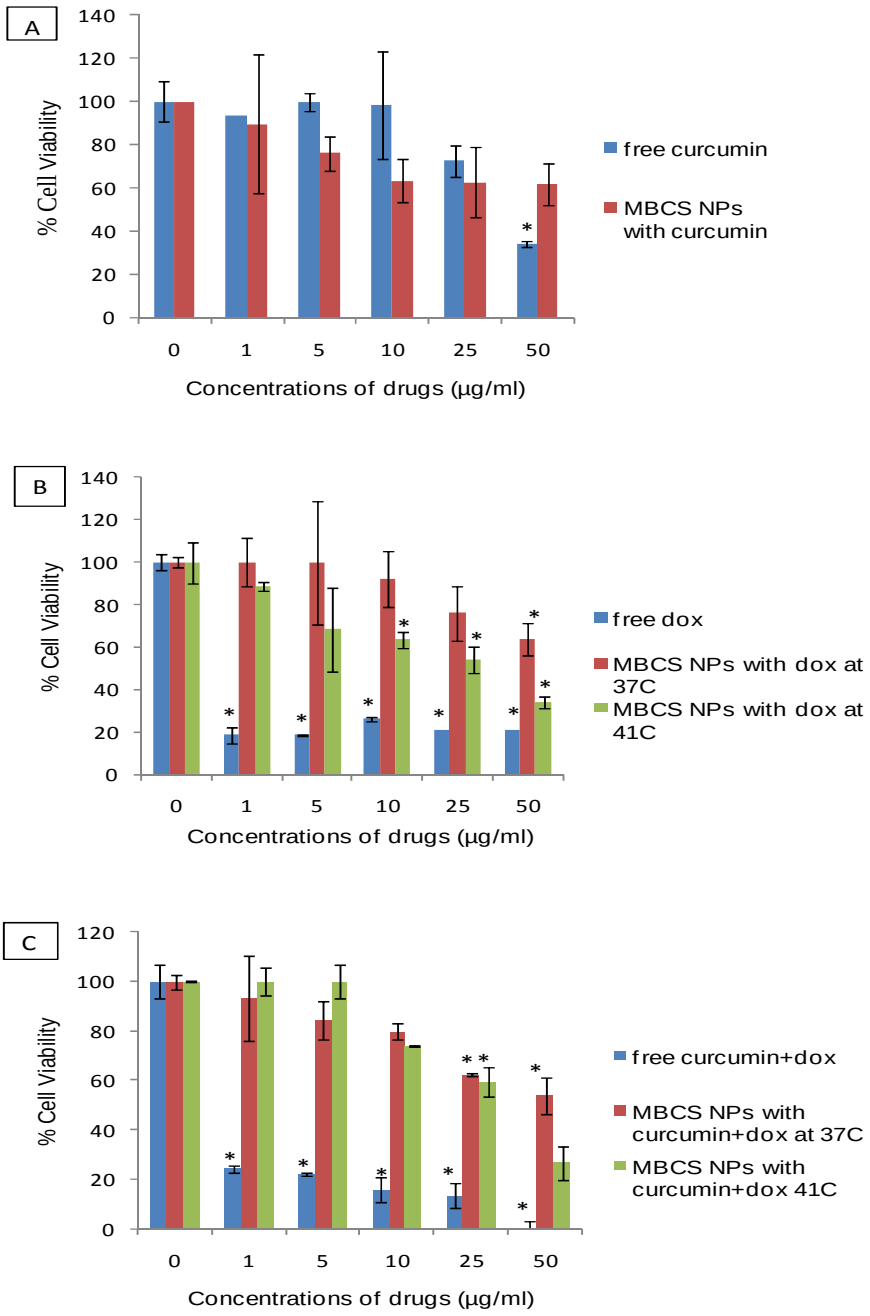

Figure 2.10 Pharmacokinetic Study in a dose dependent manner [A] Comparison of free curcumin and MBCS NPs loaded with curcumin on B16F10 cell viability [B] Comparison of free doxorubicin and MBCS NPs loaded with doxorubicin (37˚C & 41˚C) on B16F10 cell viability [C] Comparison of combination of free curcumin & doxorubicin with MBCS NPs loaded with curcumin and doxorubicin in the core and shell of the nanoparticles respectively (37˚C & 41˚C)

2.4.9 HDF cells viability study

The viability of HDF cells was assessed after interaction with the MBCS NPs at various concentrations for 24 hours using MTS assays. The results up to concentrations of 500µg/ml showed no significant toxicity. The cell viability was around 85-90% for all of the concentrations studies (Figure 2.10). The results suggest that our MBCS NPs are relatively biocompatible to the healthy cells as compared to bare magnetic nanoparticles, whose toxicity has been an issue of consideration for applications in drug delivery systems, especially at high concentrations [59, 60].

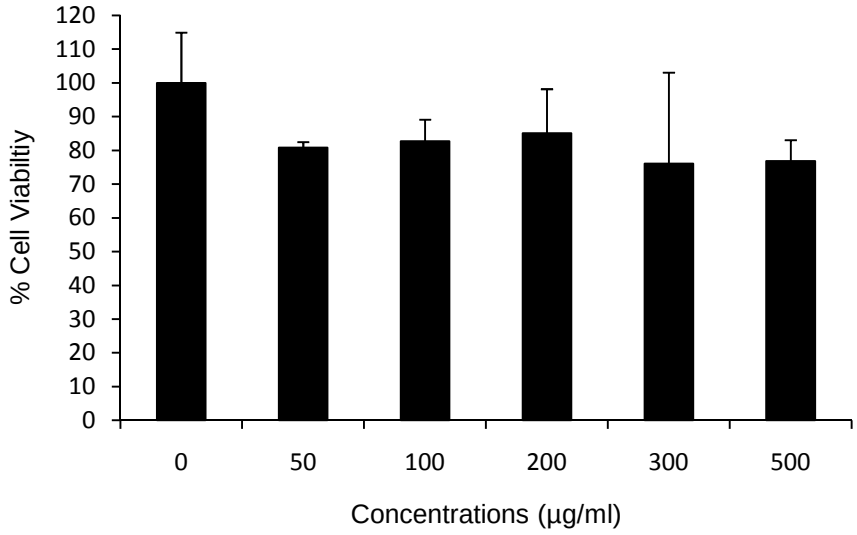

Figure 2.11 A dose dependent Cytotoxicity Study of MBCS NPs on exposure to HDF cells for 24 hours

2.4.10 Efficiency of MBCS NP uptake by B16F10 cells

In order to determine the optimal concentration of MBCS NPs that can be uptaken by our target melanoma (B16F10) cells, iron and DNA assays were done as described in section 2.3.9. The results indicate a dose dependent uptake of the nanoparticles by B16F10 cells. The uptake of nanoparticles reaches a plateau at the concentration of 300µg/ml as shown in Figure 2.11. Thus for all the cell based studies, we selected the 300µg/ml as it was the optimum concentration of nanoparticles. These results are consistent with earlier findings on different magnetic based

thermo-sensitive nanoparticles from our group which are formulated using magnetic nanoparticles as a core and temperature-sensitive polymers as a shell [56].

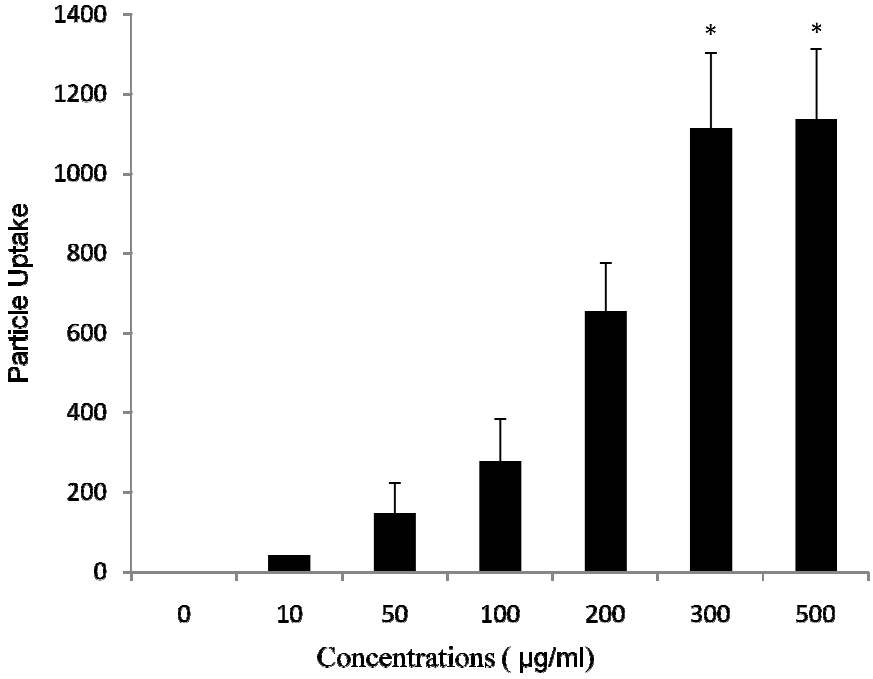

Figure 2.12 MBCS NPs uptake by B16F10 cells at various nanoparticle concentrations, * indicates significant value ($p<0.05$ for $n=4$)

2.4.11 Visualization of nanoparticle uptake by B16F10 cells

The uptake of MBCS NPs by melanoma (B16F10) cells was visualized by Prussian blue staining, which stained the iron oxide nanoparticles blue in color. As seen in Figure 2.12(C), the presence of iron oxide throughout the B16F10 cell membrane is evident suggesting that these MBCS NPs can be effectively uptaken by the cells. The control cells, which were not exposed to nanoparticles, show no presence of blue color in the cells (Figure 2.12(A)). Counter staining of the cells in pink color show the contrast, especially for cells uptaken MBCS NPs (Figure 2.12(D) Versus 2.12(B)).

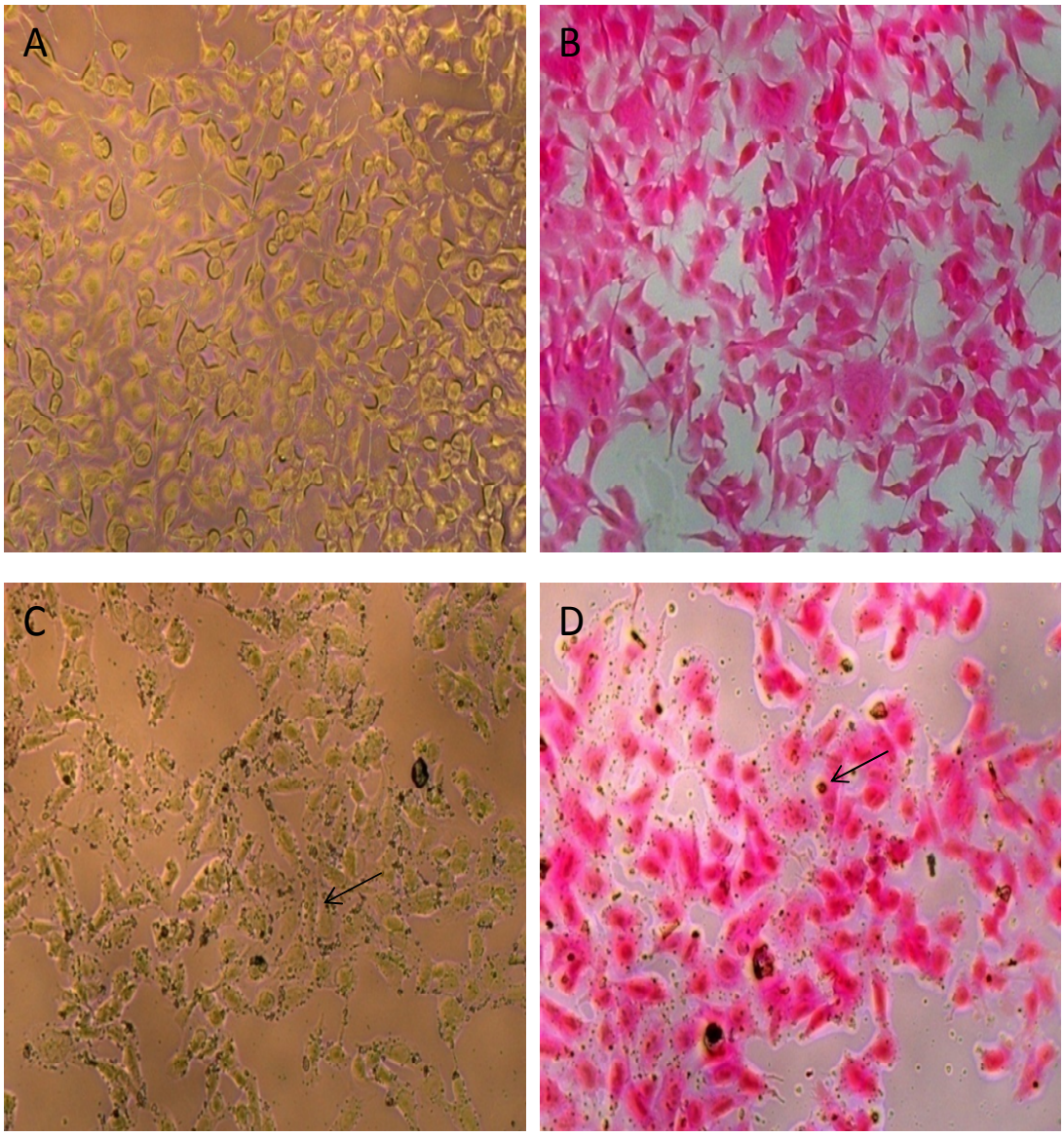

Figure 2.13 Prussian blue staining of the MBCS NPs uptaken by B16F10 cells. (A) B16F10 cells not exposed to MBCS NPs and stained with prussian blue, (B) B16F10 cells not exposed to MBCS NPs and counter stained, (C) MBCS NPs uptaken by B16F10 cells; stained with Prussian blue and (D) MBCS NPs uptaken by B16F10 cells (stained with Prussian blue with cell membrane counter stained (pink)

2.4.12 In vitro Magnetic Resonance Imaging (MRI) of MBCS NPs

The MRI studies on agarose phantoms containing MBCS NPs exhibit a higher contrast as compared to all the controls. As noted in Figure 2.13, the contrast is greatest for the higher concentration of MBCS NPs. Thus these nanoparticles can be used as contrast agents for MRI. In order to test the usefulness of MBCS NPs as MRI contrast agents when internalized by cancer

cells, the agarose phantoms containing MBCS NPs uptaken by cancer cells were also analyzed. The result in Figure 2.13(F) shows an intense contrast of cells uptaken MBCS NPs as compared to phantom consisting of cancer cells only (Figure 2.13(D)), cancer cells uptaken PLGA nanoparticles (Figure 2.13(E)). Therefore, the optimal concentration of MBCS NPs, which were effectively uptaken by the melanoma cells also gave a good contrast for MRI suggesting that our nanoparticles can also be used for real-time tracking of tumors by MRI during melanoma treatment as similar to other studies using magnetic-based nanoparticles [40, 61].

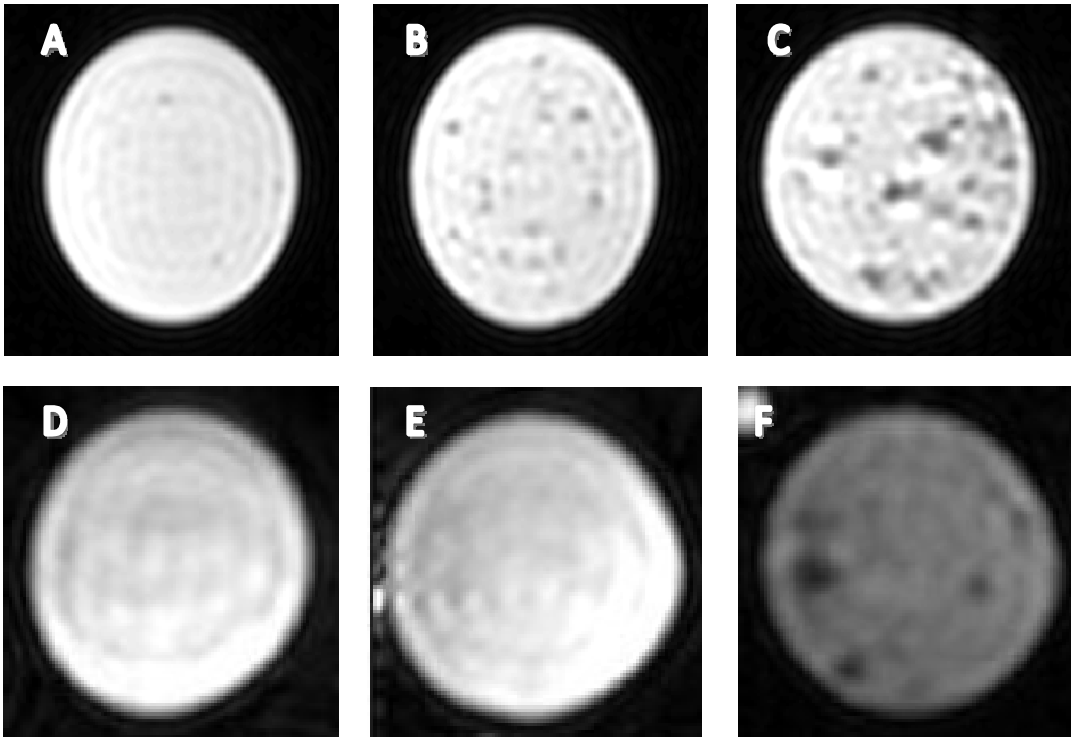

Figure 2.14 Agarose phantom images: (A) PLGA nanoparticles (0.33 mg/ml), (B) MBCS NPs (0.33 mg/ml), (C) MBCS NPs (0.66 mg/ml), (D) Melanoma cells (B16F10), (E) B16F10 cells uptaken PLGA nanoparticles, and (F) B16F10 cells uptaken MBCS NPs

2.5 Conclusion

In this chapter we have shown that we have successfully synthesized the designed MBCS NPs and characterized them using several techniques towards the fulfillment of Aim 1. The synthesized MBCS NPs contained around 15% (w/w) magnetite nanoparticles. These

nanoparticles possessed a core-shell structure, were stable, and possessed required functional groups as identified by DLS, zeta potential, magnetic property of the magnetite was decreased severely in the MBCS NPs but still within the range useful for physiological magnetic targeting applications. The curcumin release from core was sustained for a period of 25 days, while rapid burst doxorubicin release from the thermo-sensitive shell at 41˚C was observed for a period of 7 days. The cellular studies indicate biocompatibility of the MBCS NPs to the healthy cells; HDF cells and efficient dose-dependent uptake by murine melanoma (B16F10) cells. The MRI studies exhibit the potential application of the MBCS NPs for tracking of tumors for diagnosis and treatment of melanoma skin cancer.

CHAPTER 3

IN VITRO AND PRELIMINARY *IN VIVO* STUDIES OF TARGETED NANOPARTICLES

3.1 Introduction

In the previous chapter, we successfully synthesized and characterized Magnetic-Based Core-Shell Nanoparticles (MBCS NPs). The nanoparticles exhibited dual drug release, provided magnetic properties, and MRI capabilities for melanoma treatment and tracking. However, there is a need for active melanoma targeting strategy, especially targeting the drug to only cancer cells. Of all the targeting moieties such as antibodies, peptides, aptamers, and so on, targeting peptides have exhibited favorable properties like their smaller sizes compared to antibodies, ability to escape detection by RES system, and chemical stability thereby resulting in successfully targeting the nanoparticles to the cancer site [17]. Thus with the goal of increasing the target specific targeting treatment and imaging capability of the nanoparticles, we incorporated therapeutic targeting peptide Gly-Arg-Gly-Asp-Ser (GRGDS) onto MBCS nanoparticles. GRGDS is an RGD based pentapeptide known to possess anti-cell adhesive properties against B16F10 murine melanoma [62]. This peptide interacts with the $\alpha_v\beta_3$ integrin receptors overexpressed by metastatic melanoma and tumor endothelial cells making it useful for active targeting of metastatic melanoma [48]. Along with targeting efficiency, these peptides block the adhesion of murine melanoma cells i.e (B16F10 cells) to the cells of the target organs, thus inhibiting the metastasis of melanoma [63]. In this chapter, we present the conjugation scheme of GRGDS to MBCS nanoparticles (Figure 3.1) and its efficiency by *in vitro* and preliminary *in vivo* studies.

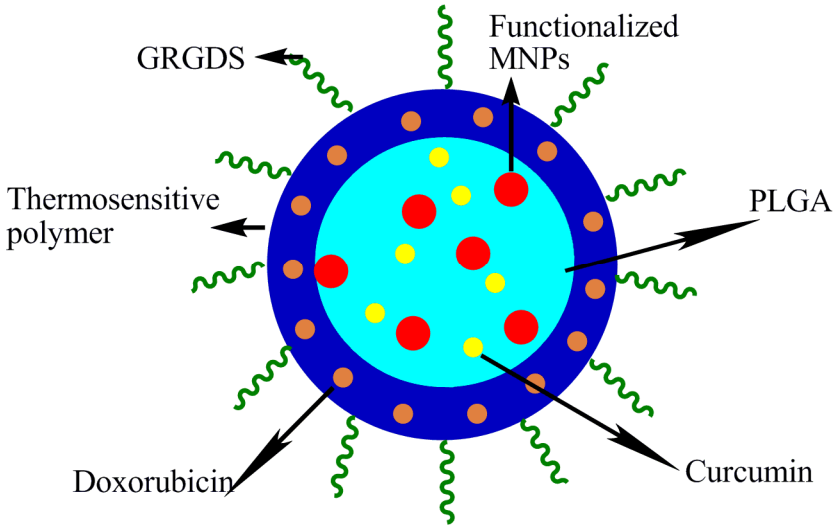

Figure 3.1 Design scheme of GRGDS-conjugated MBCS NPs

3.2 In vitro studies

3.2.1 Materials

GRGDS peptide (Anaspec), N-(3-Dimethylamineopropyl)-N'-ethylcarbodiimide hydrochloride (EDC, SIGMA), N-Hdroxy-succinimide (NHS, 98%, Aldrich), Prussian blue staining kit (Sigma-Aldrich) MES, endocytotic inhibitors (chlorpromazine, Filipin III and amiloride) (Sigma-Aldrich) and OCT compound (Tissue Tek) were purchased and used without further purification. Cardiogreen dye (ICG) was a gift from Dr. Hanli Liu.

3.2.2 GRGDS peptide conjugation to MBCS NPs

The GRGDS peptide with a carboxyl (COOH) end group was conjugated to NH_2 functional group presented on the PNIPAAm-AAm-AH tripolymeric shell of the MBCS NPs by EDC/NHS chemistry as described in Figure 3.2.

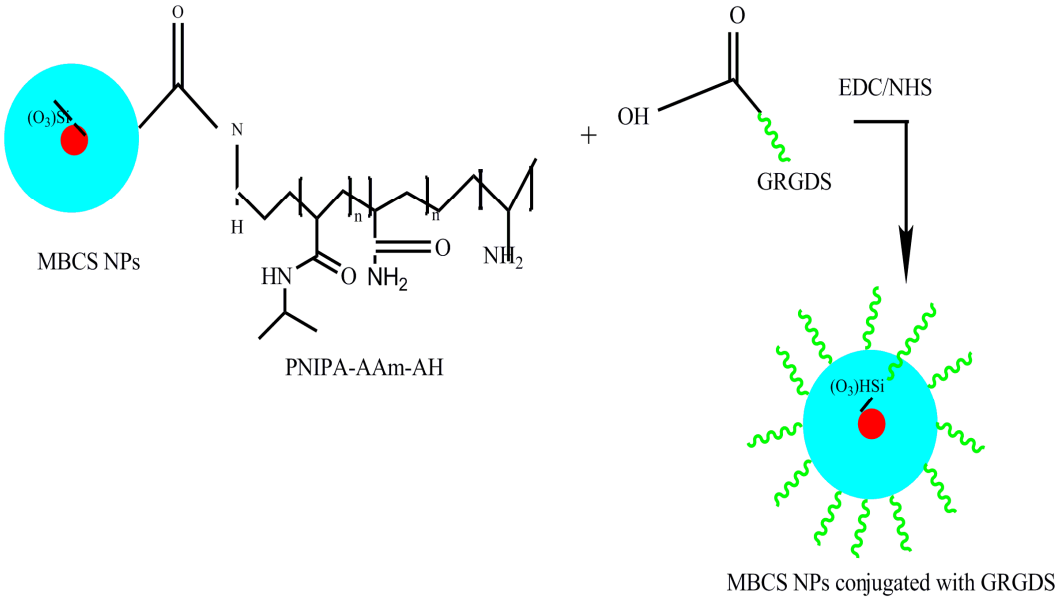

Figure 3.2 Conjugation of GRGDS peptides to MBCS NPs

3.2.3 Dynamic light scattering (DLS) and zeta potential measurement

MBCS NPs were conjugated to GRGDS, lyophilized and resuspended into DI water (0.5 mg/ml). The sample was analyzed for measurement of size, polydispersity and surface charge by Zeta potential analyzer.

3.2.4 Peptide conjugation confirmation by FTIR

To confirm the conjugation of GRGDS peptide on the MBCS NPs, FTIR spectroscopy was done on the lyophilized sample as described in section 2.3.5.

3.2.5 HDF's viability after exposure to GRGDS-conjugated MBCS NPs

GRGDS peptide has shown to induce apoptosis of the murine melanoma cells in a dose dependant manner on exposure [62]. So it was very important to access the viability of the normal healthy cells after interaction with GRGDS-conjugated MBCS NPs. Known concentrations of the nanoparticles (0, 10, 50, 100, 200, 300, and 500 µg/mL) were added to the HDF cells for an exposure time of 24 hours. The cells without addition of nanoparticles were used as controls. The cell viability was assessed by MTS assays as described in section 2.3.9.

3.2.6 Determination of mechanisms of nanoparticle uptake by B16F10 cells

To explore the mechanisms of MBCS NPs uptake by B16F10 cells, various endocytic inhibitors were used. B16F10 cells were cultured in 96-well plates overnight and the next day were pre-incubated at 37 ℃ for 1 hour with chlorpr omazine (10 µg/ml) to inhibit clathrin vesicles formation, filipin III (1 µg/ml) to hinder caveolae, and with amiloride (50 µM) to inhibit macropinocytosis. After an hour, the cells were treated with either a suspension of MBCS NPs (300 µg/ml) or of GRGDS-conjugated MBCS NPs (300 µg/ml), along with the respective inhibitors at the same concentrations, for an additional hour. At the end of the incubation time, cells were washed three times with cold PBS to remove the NPs not uptaken by the cells and then lysed by incubating them 1% Triton X-100 for 30 minutes at 37℃. The cell lysate was then quantified for the amount of iron oxide by iron assays and the results were normalized by measurement of total DNA content for all the samples by DNA picogreen assays as described in section 2.3.1.

3.2.7 Statistical Analysis

Results obtained were analyzed using one way ANOVA with $p < 0.05$ and Bonferroni Post-hoc tests (GraphPad Prism version 5.02 for Windows). All the results were presented as mean ± SD.

3.3 Preliminary *In vivo* biodistribution studies

3.3.1 Tumor growth in nude mouse

All animal experiments were performed in accordance with the animal welfare policy and IACUC approved protocols of the University of Texas at Arlington. C57/BL6 male mouse (n=1) was shaved and anesthetized using isoflurane gas followed by inoculation with 10^6 Melanoma (B16F10) cells at right shoulder and left flank each subcutaneously for growing tumors. The tumor growth was monitored regularly by vernier calipers measurement for 10 days before starting the experiment. For the experiment, a mouse in which no tumor was injected and no

nanoparticles were injected acted as a control. The final volumes of tumors were 1259 mm^3 on the right shoulder and 541 mm^3 on the left flank at the time of nanoparticle injection.

3.3.2 Intravenous injection of MBCS NPs in nude mice

The previously prepared MBCS NPs were loaded with NIR dye cardiogreen (ICG) in the PNIPAAm-AAm-AH shell of the nanoparticles as mentioned in section 2.3.8. and further conjugated with GRGDS as mentioned in section 3.2.2. After growth of tumors for about 10 days, 100 µL of the GRGDS-conjugated MBCS NPs loaded with ICG were injected intravenously at a concentration of 10 mg/ml in sterile PBS via tail vein injection. For the first hour of the nanoparticles circulation, a neodymium permanent magnet of 2451 Gauss surface field was affixed on the tumor in the shoulder region to quantify the effect of magnetic attraction of MBCS NPs to the tumor site.

3.3.3 NIR Imaging for bio-distribution monitoring

The *in vivo* biodistribution of the MBCS NPs was monitored after 1, 2, 6 and 24 hours post injection. The mouse was anesthetized at each time and then imaged under KODAK FX Pro imaging system (Carestream). After 24 hours the control and sample mice were sacrificed by giving an overdose of CO_2 and their major organs like heart, lungs, liver, kidneys, spleen and tumors were harvested and washed with cold PBS to remove the blood. The sample and control organs were imaged in the imaging system and their normalized fluorescent intensities were compared (MATLAB) to determine the biodistribution of the GRGDS-conjugated MBCS NPs.

3.4 Results and discussion

3.4.1 Nanoparticle size, polydispersity and zeta potential

On conjugation of the MBCS NPs to GRGDS, the average particle size was increased from 296 nm to 399 nm (Table 3.1). The net surface charge of the nanoparticles after conjugation became more negative, and that might be due to the presence of cationic carboxylic acid groups of the peptides.

Table 3.1 Nanoparticle size, polydispersity, and surface charge (zeta potential) after peptide conjugation.

Sample	Size (nm)	Polydispersity	Zeta potential (mV)
MBCS NPs (PLGA-MNPSi-AH-tripolymer nanoparticles)	296.0 ± 15.2	0.278 ± 0.018	-12.07 ± 0.18
GRGDS-conjugated MBCS NPs	398.7 ± 6.15	0.338 ± 0.006	-21.09 ± 1.18

3.4.2 Confirmation of GRGDS peptide conjugation on MBCS NPs

The comparison of the FTIR spectra of the MBCS NPs and GRGDS-conjugated MBCS NPs is illustrated in Figure 3.3. The presence of broad and intense spectra of the primary amide I in the range of 1650-1750 cm^{-1} associated with the carbonyl (C=O) stretching of the amide, and amide II bands in the range of 1450-1550 cm^{-1} associated with (N-H) stretching of the amide, which were characteristics of peptide conjugation. These results are synonymous with results reported elsewhere using GRGDS peptides [64, 65].

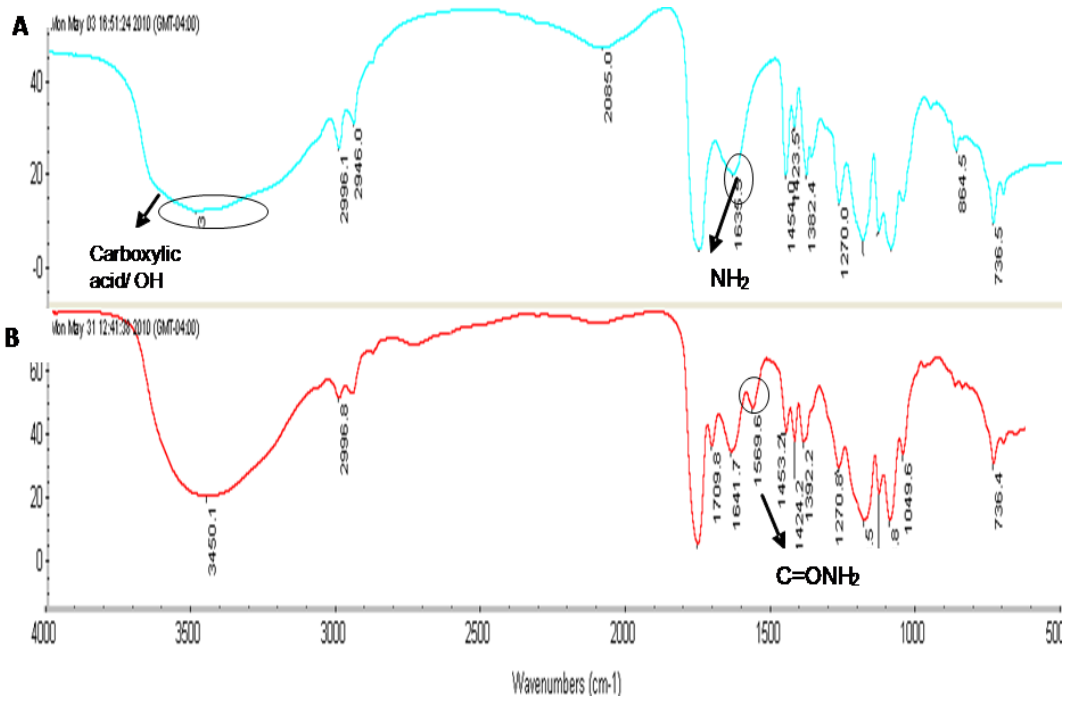

Figure 3.3 FTIR spectrum of (A) MBCS NPs and (B) GRGDS-conjugated MBCS NPs

3.4.3 Effect of GRGDS-conjugated MBCS NPs on HDF viability

From the results in Figure 3.4 it can be proved that the GRGDS-conjugated nanoparticles are compatible with the HDF cells. The cell viability was around 90% for nanoparticle concentrations upto 500µg/ml. Thus we can establish that peptide-conjugated nanoparticles would not cause any harmful effects on the healthy cells.

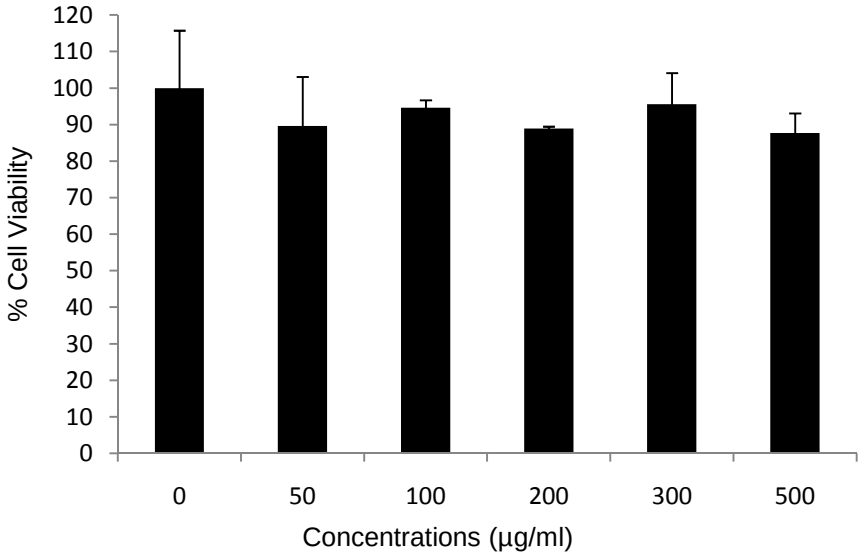

Figure 3.4 HDF cell viability on exposure to GRGDS-conjugated MBCS NPs at various doses (n=4)

3.4.4 Mechanism of nanoparticle uptake into B16F10 cells

The mechanism by which the MBCS NPs and GRGDS-conjugated MBCS NPs were internalized by cancer cells was identified using the endocytotic inhibitors, which blocked the activity of caveolae buds, clathrin coated pits, and macropinocytotic pathways. Cellular uptake of MBCS NPs exhibited a 60% reduction when the caveolae pathways were blocked (Figure 3.5) where as the uptake reduction was 80% for the GRGDS-conjugated MBCS NPs. These results suggest that caveolae pathways are the most important pathway for the internalization of MBCS NPs, especially peptide-conjugated nanoparticles. This result can be co-related to the function of caveolae buds which have been shown to play most important role in different ligand-receptor based endocytosis. For the clathrin inhibited pathways, MBCS NPs uptake was reduced by 40% and GRGDS-conjugated MBCS NPs uptake was reduced by 60%. Macropinocytosis inhibition reduced the uptake of both the types of nanoparticles by 55-60%. The individual as well as combined effect of all the 3 endocytotic inhibitors reduced the intracellur uptake efficiency as observed from our results [66].

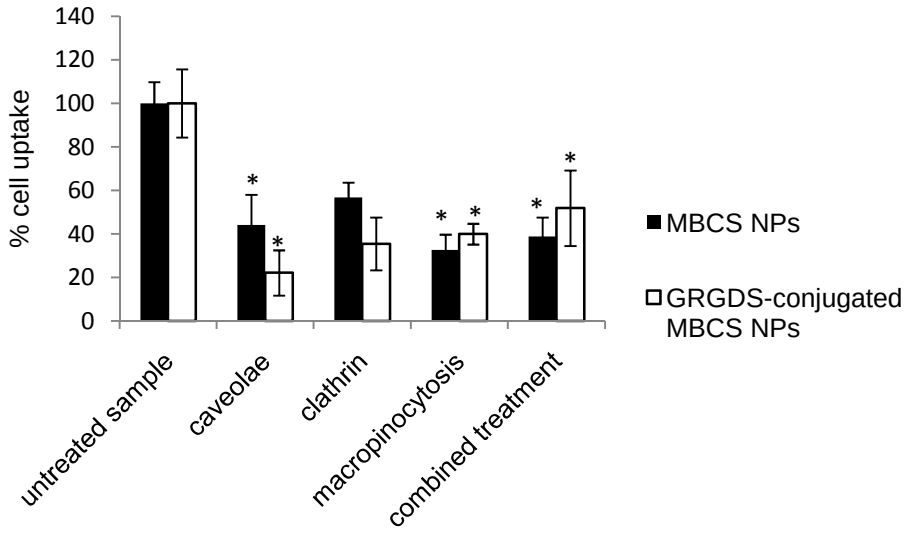

Figure 3.5 Uptake mechanisms of MBCS NPs and GRGDS-conjugated MBCS NPs by B16F10 cells study using different endocytotic pathway inhibitors, * $p < 0.05$ as compared to control (n=3)

3.4.5 Bio-distribution of GRGDS-conjugated MBCS NPs by NIR imaging

The distribution pattern of GRGDS-conjugated nanoparticles after intravenous injection was determined by NIR imaging. At 1, 2, 6, and 24 hrs post injection the mouse was imaged, and the results were shown in Figure 3.6. After one hour, the nanoparticle deposition in liver, kidneys, and surrounding areas is observed. The intensity in liver, kidneys and lungs becomes stronger at each time point. The recruitment of the nanoparticles at both the tumor sites intensifies with increase in time as shown in Figure 3.6 (H, I, and J). The presence of nanoparticles in the tumor is clearly seen in the *ex vivo* images in Figure 3.7 and Figure 3.8 but the intensity is low in tumors compared to the intensity of nanoparticles in lungs, liver and kidneys.

The clearance and biodistribution of the polymeric/metallic nanoparticles is dependent on various factors like nanoparticles size, surface charge, hydrophilicity/hydrophobicity, and targeting strategies used. As our nanoparticles size is in the range of 400 nm, the uptake of the nanoparticles by macrophages leading to the particle accumulation in liver and kidneys was expected [67]. The localization of nanoparticles in the tumor can be attributed to the GRGDS-conjugation as active strategies have been shown successful targeting results in the past [68].

Also, the highly negative charge on the surface of GRGDS-conjugated MBCS NPs may have decreased non-specific uptake and longer circulation time leading to the accumulation of nanoparticles in tumor regions [69]. The effect of an external magnetic field was negligible in tumor homing as there is not much difference in the nanoparticle accumulation at both tumor sites. These results are similar to other studies using similar type of external magnetic fields for nanoparticle recruitment [35].

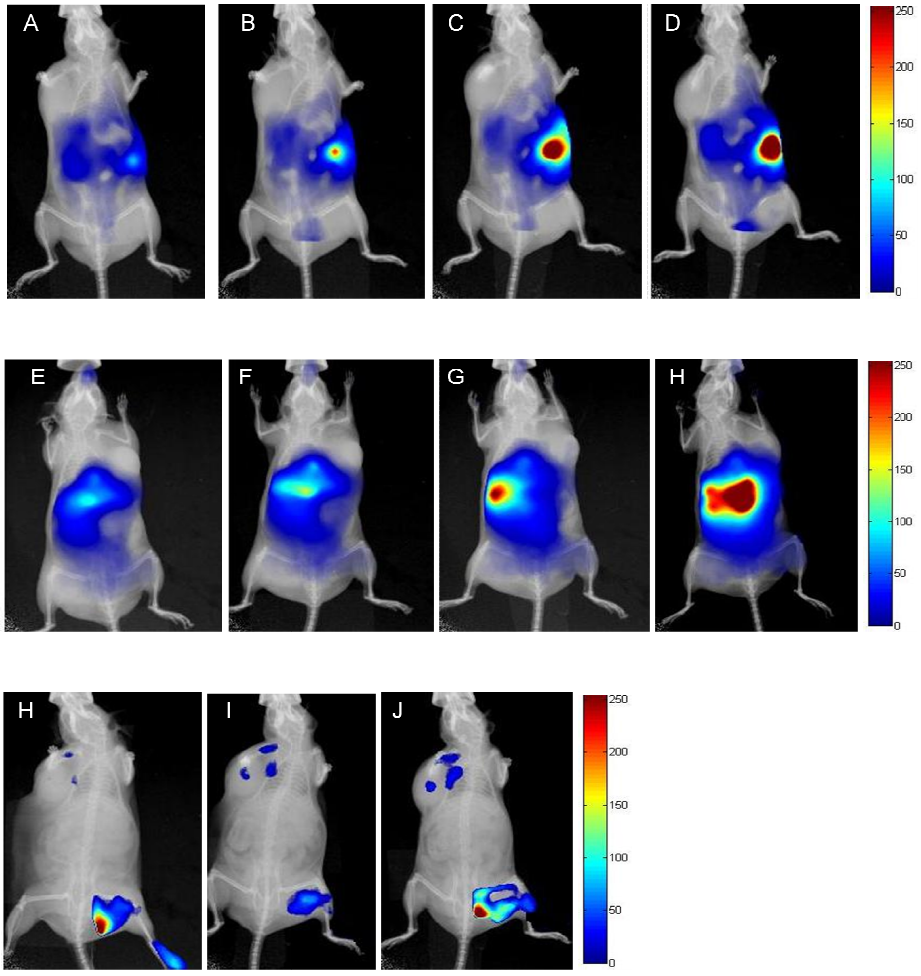

Figure 3.6 *In vivo* imaging of the mouse after intravenous injection of GRGDS-conjugated MBCS NPs. Figures A,B,C,D are dorsal view images for 1, 2, 6, and 24 hrs respectively; Figures E,F,G, and H are ventral view images for 1, 2, 6, and 24 hrs respectively; Figures I, J, K are dorsal view images with only tumors exposed at 2,6, and 24 hours respectively

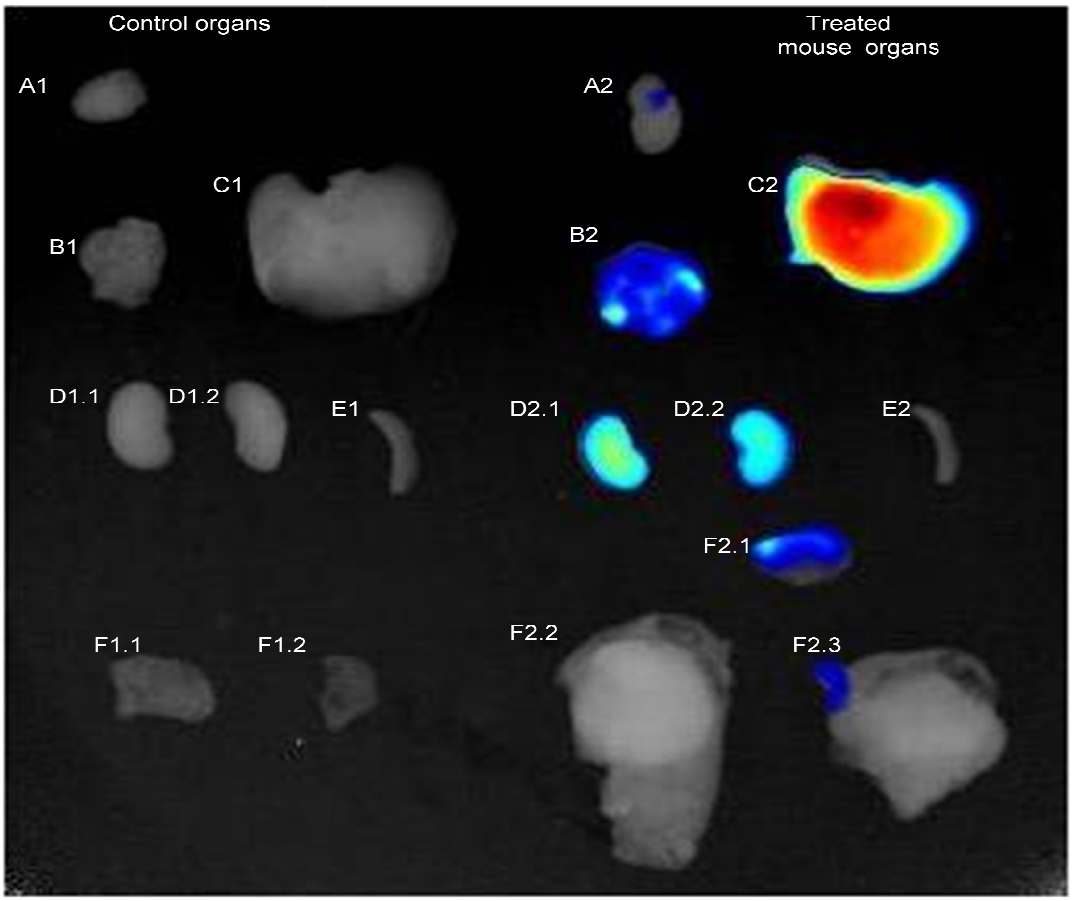

Figure 3.7 Ex-vivo imaging of organs of control and treated mouse. Left side indicates control organs and the right size of the image indicates treated mouse organs (A1 and A2-heart), (B1 and B2-lung), (C1 and C2-liver), (D1.1, 1.2, 2.1, 2.2-kidneys), (E1 and E2- spleen), (F1.1 and F1.2-skin from shoulder and leg respectively for the control mouse, F2.1 is skin from abdomen of the treated mouse, F2.2 and F2.3 are the tumors from shoulder & leg respectively of the treated mouse)

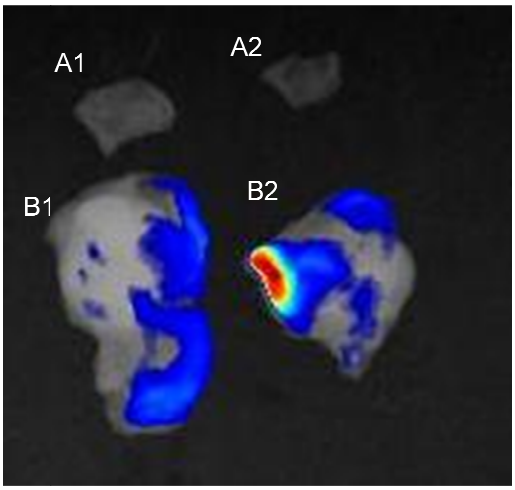

Figure 3.8 *Ex vivo* imaging of skin from control mouse and tumors from treated mouse (A1-shoulder skin from control mouse, A2-leg skin from control mouse, B1-shoulder tumor in treated mouse, B2-leg tumor in treated mouse)

Figure 3.9 *Ex vivo* comparison of fluorescence intensities from different organs of controlled and treated mouse

3.5 Conclusion

In this chapter, we successfully synthesized GRGDS-conjugated MBCS NPs, characterized them for particle size, zeta potential, and confirmed the peptide conjugation by FTIR spectroscopy. The GRGDS-conjugated MBCS NPs exhibited biocompatibility to the HDF cells upto a concentration of 500 µg/ml. The uptake of the nanoparticles was mainly dependent

on the receptor ligand-based endocytosis for peptide conjugated nanoparticles. The preliminary *in vivo* biodistribution results indicate major depositions of the nanoparticles in liver, kidneys and lungs which was around two-fold higher than the nanoparticle depositions in tumors. The effect of external magnetic field on nanoparticles recruitment in the tumor sites was negligible. For further increasing the system efficiency, few limitations and some alternatives are suggested in the chapter 4.

CHAPTER 4

SUMMARY, LIMITATIONS, AND FUTURE WORK

In the work presented, we successfully developed Magnetic-based Core-Shell Nanoparticles (MBCS NPs) and characterized them for several properties important for drug delivery-based applications for cancer therapy. The core-shell structure of the nanoparticles provided the encapsulation of magnetic nanoparticles into the biodegradable polymeric core, thus eliminating toxicity and aggregation issues associated with several magnetic nanoparticles while preserving their magnetic properties of attraction. Also the presence of biodegradable core provided an efficient cargo for sustained drug release applications for a long-term cancer treatment. The drug release study from thermo-sensitive shell of these nanoparticles supported their potential use for controlled release of drugs in response to changes in temperature along with hyperthermia treatment. The developed MBCS NPs exhibited excellent biocompatibility to the healthy cells and efficiency of being uptaken by the target cancer cells. The MBCS NPs also displayed a great potential to be used as imaging probes for a real-time tumor tracking using non invasive MR imaging modalities.

The overall strategy seemed to be promising for melanoma treatment to increase the system efficiency and selectivity, the MBCS NPs were further conjugated with therapeutic targeting peptides GRGDS. The GRGDS-conjugated MBCS NPs were also found to be biocompatible to the healthy cells. In addition, the uptake of these nanoparticles was mainly dependent on receptor mediated endocytotic processes, which were illustrated in the uptake mechanism study. The preliminary *in vivo* studies exhibited almost equal depositions of the nanoparticles at both tumors irrespective of the application of an external magnet on the surface of the tumor, leading to a conclusion that the deposition of nanoparticles at the tumor site was due to the peptide targeting strategy and there was no positive effect of an external magnetic field

on the recruitment of the nanoparticles. Other reason is due to the location of the magnet is at the shoulder, whereas the tumor site at the leg was used for a control without exposure to a magnet. The recruitment of the nanoparticles was similar at both the tumor sites and this might be due to longer travel distance for particles to reach to the shoulder than the legs. Greater depositions of the GRGDS-conjugated MBCS NPs were found in the organs like liver, kidneys, and lungs as compared to tumor depositions which requires further investigations and few improvements suggested below.

Though the characterization, cellular studies, and preliminary *in vivo* studies exhibited positive results, few limitations of the system were recognized.

- The size of the MBCS NPs is in the range of 300-400 nm which might have resulted in the increased deposition of the nanoparticles in the organs of the RES system. Thus in future the particle size should be tried to be reduced by sophistication of the synthesis procedures.

- The magnetic property of the MBCS NPs lies in the desired range for drug delivery based applications but the strength of an external magnetic field suitable for magnetic drug targeting for our MBCS NPs should be determined for precise control to reach the effectiveness of the working system *in vitro* and *in vivo*.

- The presence of functional groups on the surface of the MBCS NPs may be little for GRGDS conjugation resulting in decrease in the active targeting efficiency of the particles. Thus the number of functional groups present on the nanoparticles should be assessed before and after peptide conjugation. If this is the case, more functional groups should be introduced (for example, the use of avidin and biotin has been used to increase functional groups for bioconjugation.

Future work for this project will include the following studies:

- Analysis of effects of different external magnetic fields on attraction of our MBCS NPs and determination of the ideal magnetic field for our targeting applications.
- Effects of the dual drug release combined with the therapeutic efficiency of the peptide on the tumor growth and metastasis *in vivo* using MR imaging techniques.
- *In vitro* and *In vivo* treatment studies using dual drug delivery approach of our nanoparticles on cell lines resistant to a conventional chemotherapy.

REFERENCES

1. *Skin cancer*, in *MedilinePlus*, J. Kantor, Editor. 2009.

2. Nestle, F.O., G. Burg, and R. Dummer, *New perspectives on immunobiology and immunotherapy of melanoma.* Immunology Today, 1999. **20**(1): p. 5-7.

3. Gupta, S. and H. Mukhtar, *Chemoprevention of Skin Cancer: Current Status and Future Prospects.* Cancer and Metastasis Reviews, 2002. **21**(3): p. 363-380.

4. Brash, D.E., et al., *A role for sunlight in skin cancer: UV-induced p53 mutations in squamous cell carcinoma.* Proceedings of the National Academy of Sciences of the United States of America, 1991. **88**(22): p. 10124-10128.

5. *Skin cancer*. Available from: http://www.mayoclinic.com/health/skin-cancer/ds00190.

6. *Skin cancer*. 2010; Available from: http://www.cdc.gov/cancer/skin/statistics/index.htm.

7. Fidler, I.J., *The pathogenesis of cancer metastasis: the 'seed and soil' hypothesis revisited.* Nat Rev Cancer, 2003. **3**(6): p. 453-458.

8. *MoonDragon's Health & Wellness; skin cancer*. Available from: http://www.moondragon.org/health/disorders/skincancer.html.

9. *Skin Cancer Treatment*. Available from http://www.cancer.gov/cancertopics/pdq/treatment/skin/Patient.

10. *Skin Cancer Facts*. 2009; Available from: http://www.cancer.org/docroot/ped/content/ped_7_1_what_you_need_to_know_about_skin_cancer.asp.

11. Yang, X., et al., *Preparation of magnetite and tumor dual-targeting hollow polymer microspheres with pH-sensitivity for anticancer drug-carriers.* Polymer. **51**(12): p. 2533-2539.

12. Veiseh, O., J.W. Gunn, and M. Zhang, *Design and fabrication of magnetic nanoparticles for targeted drug delivery and imaging.* Advanced Drug Delivery Reviews. **62**(3): p. 284-304.

13. Shubayev, V.I., T.R. Pisanic Ii, and S. Jin, *Magnetic nanoparticles for theragnostics.* Advanced Drug Delivery Reviews, 2009. **61**(6): p. 467-477.

14. Odot, J., et al., *In vitro and in vivo anti-tumoral effect of curcumin against melanoma cells.* International Journal of Cancer, 2004. **111**(3): p. 381-387.

15. Torchilin, V.P., *Multifunctional nanocarriers.* Advanced Drug Delivery Reviews, 2006. **58**(14): p. 1532-1555.

16. Sun, C., J.S.H. Lee, and M. Zhang, *Magnetic nanoparticles in MR imaging and drug delivery.* Advanced Drug Delivery Reviews, 2008. **60**(11): p. 1252-1265.

17. Aina, O.H., et al., *Therapeutic cancer targeting peptides.* Peptide Science, 2002. **66**(3): p. 184-199.

18. Sinha, R., et al., *Nanotechnology in cancer therapeutics: bioconjugated nanoparticles for drug delivery.* Molecular Cancer Therapeutics, 2006. **5**(8): p. 1909-1917.

19. Fan, L., et al., *Co-delivery of PDTC and doxorubicin by multifunctional micellar nanoparticles to achieve active targeted drug delivery and overcome multidrug resistance.* Biomaterials. **31**(21): p. 5634-5642.

20. Kumari, A., S.K. Yadav, and S.C. Yadav, *Biodegradable polymeric nanoparticles based drug delivery systems.* Colloids and Surfaces B: Biointerfaces. **75**(1): p. 1-18.

21. Shaikh, J., et al., *Nanoparticle encapsulation improves oral bioavailability of curcumin by at least 9-fold when compared to curcumin administered with piperine as absorption enhancer.* European Journal of Pharmaceutical Sciences, 2009. **37**(3-4): p. 223-230.

22. Jarzyna, P.A., et al., *Iron oxide core oil-in-water emulsions as a multifunctional nanoparticle platform for tumor targeting and imaging.* Biomaterials, 2009. **30**(36): p. 6947-6954.

23. Chung, Y.-I., et al., *The effect of surface functionalization of PLGA nanoparticles by heparin- or chitosan-conjugated Pluronic on tumor targeting.* Journal of Controlled Release. **143**(3): p. 374-382.

24. Butoescu, N., et al., *Dexamethasone-containing biodegradable superparamagnetic microparticles for intra-articular administration: Physicochemical and magnetic properties, in vitro and in vivo drug release.* European Journal of Pharmaceutics and Biopharmaceutics, 2009. **72**(3): p. 529-538.

25. Yu, F., et al., *The magnetophoretic mobility and superparamagnetism of core-shell iron oxide nanoparticles with dual targeting and imaging functionality.* Biomaterials. **31**(22): p. 5842-5848.

26. Prashant, C., et al., *Superparamagnetic iron oxide - Loaded poly (lactic acid)-d-[alpha]-tocopherol polyethylene glycol 1000 succinate copolymer nanoparticles as MRI contrast agent.* Biomaterials. **31**(21): p. 5588-5597.

27. Catherine C. Berry, S.W., Stuart Charles, and Adam S. G. Curtis, *POTENTIAL DRUG - CELL DELIVERY ROUTES USING MAGNETIC NANOPARTICLES.* European Cells and Materials, 2003. **6**.

28. Lee, S.-J., et al., *Nanoparticles of magnetic ferric oxides encapsulated with poly (D,L latide-co-glycolide) and their applications to magnetic resonance imaging contrast agent.* Journal of Magnetism and Magnetic Materials, 2004. **272-276**(Part 3): p. 2432-2433.

29. Lee, S.-J., et al., *Magnetic enhancement of iron oxide nanoparticles encapsulated with poly(d,l-latide-co-glycolide).* Colloids and Surfaces A: Physicochemical and Engineering Aspects, 2005. **255**(1-3): p. 19-25.

30. N. Arsalani, H.F., M.Nazarpoor, *Synthesis and characterization of PVP-functionalized superparamagnetic Fe_3O_4 nanoparticles as an MRI contrast agent.* eXPRESS Polymer Letters, 2010. **4**(6): p. 329-338.

31. Sun, L., et al., *A biocompatible approach to surface modification: Biodegradable polymer functionalized super-paramagnetic iron oxide nanoparticles.* Materials Science and Engineering: C. **30**(4): p. 583-589.

32. Wang, Z., W.-K. Chui, and P. Ho, *Design of a Multifunctional PLGA Nanoparticulate Drug Delivery System: Evaluation of its Physicochemical Properties and Anticancer Activity to Malignant Cancer Cells.* Pharmaceutical Research, 2009. **26**(5): p. 1162-1171.

33. Martin, A., et al., *Synthesis of bombesin-functionalized iron oxide nanoparticles and their specific uptake in prostate cancer cells.* Journal of Nanoparticle Research. **12**(5): p. 1599-1608.

34. Ruirui Qiao, C.Y.a.M.G., *Superparamagnetic iron oxide nanoparticles: from preparations to in vivo MRI applications.* Journal of Materials Chemistry, 2009. **19**.

35. Stella Chiu, N.P.G. *Magnetically Targeted Iron Oxide Nanoparticle Biodistribution in C3H Mice*.

36. Balivada, S., et al., *A/C magnetic hyperthermia of melanoma mediated by iron(0)/iron oxide core/shell magnetic nanoparticles: a mouse study.* BMC Cancer. **10**(1): p. 119.

37. Phillips, J.L., *A Topical Review of Magnetic Fluid Hyperthermia.* Journal of Science & Health at the University of Alabama, 2005.

38. Barakat, N.S., *Magnetically Modulated Nanosystems: A Unique Drug-Delivery Platform: Medical Application of Functionalized MNPs.* Nanomedicine: Nanotechnology, Biology and Medicine, 2009. **4**: p. 799-812.

39. Rapoport, N., *Physical stimuli-responsive polymeric micelles for anti-cancer drug delivery.* Progress in Polymer Science. **32**(8-9): p. 962-990.

40. Rahimi, M., et al., *In vitro evaluation of novel polymer-coated magnetic nanoparticles for controlled drug delivery.* Nanomedicine: Nanotechnology, Biology and Medicine. **In Press, Corrected Proof**.

41. Gil, E.S. and S.M. Hudson, *Stimuli-reponsive polymers and their bioconjugates.* Progress in Polymer Science, 2004. **29**(12): p. 1173-1222.

42. Koppolu, B., et al., *Development of multiple-layer polymeric particles for targeted and controlled drug delivery.* Nanomedicine: Nanotechnology, Biology and Medicine. **6**(2): p. 355-361.

43. Brigger, I., C. Dubernet, and P. Couvreur, *Nanoparticles in cancer therapy and diagnosis.* Advanced Drug Delivery Reviews, 2002. **54**(5): p. 631-651.

44. Kim, K., et al., *Tumor-homing multifunctional nanoparticles for cancer theragnosis: Simultaneous diagnosis, drug delivery, and therapeutic monitoring.* Journal of Controlled Release. **In Press, Corrected Proof**.

45. Rahimi, M., et al., *Formulation and Characterization of Novel Temperature Sensitive Polymer-Coated Magnetic Nanoparticles.* Journal of Nanoscience and Nanotechnology. **10**: p. 6072-6081.

46. Gupta, A.K. and M. Gupta, *Cytotoxicity suppression and cellular uptake enhancement of surface modified magnetic nanoparticles.* Biomaterials, 2005. **26**(13): p. 1565-1573.

47. Menon, L.G., R. Kuttan, and G. Kuttan, *Inhibition of lung metastasis in mice induced by B16F10 melanoma cells by polyphenolic compounds.* Cancer Letters, 1995. **95**(1-2): p. 221-225.

48. Xiong, X.-B., et al., *Multifunctional Polymeric Micelles for Enhanced Intracellular Delivery of Doxorubicin to Metastatic Cancer Cells.* Pharmaceutical Research, 2008. **25**(11): p. 2555-2566.

49. Liu, X., et al., *Preparation and characterization of amino-silane modified superparamagnetic silica nanospheres.* Journal of Magnetism and Magnetic Materials, 2004. **270**(1-2): p. 1-6.

50. *ALS: Useful FTIR info and links*. Available from: http://infrared.als.lbl.gov/content/web-links/60-ir-band-positions.

51. *Infrared spectroscopy correlation table*. Available from: http://en.wikipedia.org/wiki/Infrared_spectroscopy_correlation_table.

52. Denizot, B., et al., *Phosphorylcholine Coating of Iron Oxide Nanoparticles.* Journal of Colloid and Interface Science, 1999. **209**(1): p. 66-71.

53. Ma, H.-l., et al., *Preparation and characterization of superparamagnetic iron oxide nanoparticles stabilized by alginate.* International Journal of Pharmaceutics, 2007. **333**(1-2): p. 177-186.

54. Brusentsov, N.A., et al., *Evaluation of ferromagnetic fluids and suspensions for the site-specific radiofrequency-induced hyperthermia of MX11 sarcoma cells in vitro.* Journal of Magnetism and Magnetic Materials, 2001. **225**(1-2): p. 113-117.

55. Xu, C., et al., *Nitrilotriacetic Acid-Modified Magnetic Nanoparticles as a General Agent to Bind Histidine-Tagged Proteins.* Journal of the American Chemical Society, 2004. **126**(11): p. 3392-3393.

56. Rahimi, M., *Magnetic Drug Targeting: Development Of A Novel Drug Delivery System For Prostate Cancer Therapy*, in *Biomedical Engineering*. 2008, University of Texas at Arlington: Arlington.

57. Koppolu, B., *Development of Novel Multilayered Particles for Drug Delivery and Cell Isolation applications*, in *Biomedical Engineering*. 2008, University of Texas at Arlington: Arlington.

58. Rahimi, M., et al., *Formulation and Characterization of a Covalently Coated Magnetic Nanogel.* Journal of Nanoscience and Nanotechnology, 2009. **9**: p. 4128-4134.

59. Mahmoudi, M., et al., *Cell toxicity of superparamagnetic iron oxide nanoparticles.* Journal of Colloid and Interface Science, 2009. **336**(2): p. 510-518.

60. Xinying Wu, Y.T., Hui Mao, *Toxic effects of iron oxide nanoparticles on human umbilical vein endothelial cells.* International Journal of Nanomedicine, 2010. **2010:5**: p. 385-399.

61. Pinkernelle, J., et al., *Imaging of single human carcinoma cells in vitro using a clinical whole-body magnetic resonance scanner at 3.0 T.* Magnetic Resonance in Medicine, 2005. **53**(5): p. 1187-1192.

62. Humphries, M.J., K.M. Yamada, and K. Olden, *Investigation of the biological effects of anti-cell adhesive synthetic peptides that inhibit experimental metastasis of B16-F10 murine melanoma cells.* The Journal of Clinical Investigation, 1988. **81**(3): p. 782-790.

63. Yang, J., et al., *Evaluation of a Novel Arg-Gly-Asp-Conjugated Î±-Melanocyte Stimulating Hormone Hybrid Peptide for Potential Melanoma Therapy.* Bioconjugate Chemistry, 2009. **20**(8): p. 1634-1642.

64. Kyung Min Park, Y.K.J., and Ki Dong Park, *RGD-Conjugated Chitosan-Pluronic Hydrogels as a Cell Supported Scaffold for Articular Cartilage Regeneration.* Macromolecular Research, 2008. **16**: p. 517-523.

65. Gallagher, W., *FTIR Analysis of Protein Structure.*

66. Nihal S. Parkar, B.S.A., Ludwig C. Nitsche, Lewis E. Wedgewood, Aaron T. Place, Maria S. Sverdlov, Oleg Chaga, and Richard D. Minshall, *Vesicle Formation and Endocytosis: Function, Machinery, Mechanisms, and Modeling.* Antioxid Redox Signal, 2009. **11**: p. 1301-1312.

67. Nagayama, S., et al.,*Time-dependent changes in opsonin amount associated on nanoparticles alter their hepatic uptake characteristics.* International Journal of Pharmaceutics, 2007. **342**(1-2): p. 215-221.

68. Danhier, F., et al., *Targeting of tumor endothelium by RGD-grafted PLGA-nanoparticles loaded with Paclitaxel.* Journal of Controlled Release, 2009. **140**(2): p. 166-173.

69. Alexis, F., et al., *Factors Affecting the Clearance and Biodistribution of Polymeric Nanoparticles.* Molecular Pharmaceutics, 2008. **5**(4): p. 505-515.

BIOGRAPHICAL INFORMATION

Zarna Bhavsar was born in Ahmedabad, India in December 1986. She pursued her Bachelor of Technology in Biomedical Engineering from Shri U.V Patel college of Engineering, Ganpath University, India, and graduated in July 2008. To fulfill the thirst for more knowledge and experience, she joined the Master of Science in biomedical engineering program at the University of Texas at Arlington in August 2008. She started conducting research in the field of drug delivery and tissue engineering under the mentorship of Dr. Kytai T Nguyen. She worked on several projects in the field of nanotechnology-based drug delivery systems for cancer therapy. She intends to continue working in a research atmosphere in the field of drug delivery systems and tissue engineering.